Correlation of Flatwise and Chordwise Bending Moments for a Sikorsky Full-Scale Bearingless Main Rotor

James M. Wang
Dynamicist

Sikorsky Aircraft Division
United Technologies Corporation
Stratford, CT

Thomas R. Norman
Aerodynamicist

Rotorcraft Aeromechanics Branch
NASA Ames Research Center
Moffett Field, CA

A study was carried out to compare the measured and analytically predicted flexbeam and blade bending moments for a modern Sikorsky bearingless main rotor. The measured data from a full-scale wind tunnel test and predicted results are presented for speeds ranging from 40 to 150 knots. Three analytical methods are used: a transfer matrix technique, a modal method, and a force summation method. Their strong points and weak points are discussed. Some of the parameters necessary for obtaining accurate predictions are identified.

Introduction

The accurate prediction of rotor vibratory loads remains a challenge for rotorcraft researchers. A prerequisite to accurate hub loads prediction is the ability to accurately predict the blade bending moments. For a bearingless rotor, which has multiple load paths and structural and kinematic couplings, the accurate prediction of bending moments in the flexbeam, torque tube and blade becomes a further challenge. The objective of this paper is to present results from a recent correlation study of flatwise and chordwise bending moments for a full-scale bearingless main rotor.

The data used were obtained from an extensive wind tunnel test (Ref. 1) of the Sikorsky proof-of-concept 5-bladed full-scale bearingless main rotor (BMR). The test was conducted in 1992 at the NASA Ames 40- by 80-Foot Wind Tunnel of the National Full-Scale Aerodynamic Complex (NFAC). This BMR is a 44-ft diameter main rotor sized for the Sikorsky S-76 helicopter. The wind tunnel test included flight conditions from 0 to 200 knots, and thrust levels from -4,000 to 18,000 lb. Parametric sweeps were conducted to systematically examine the effects of rotor speed, forward speed, thrust level, cyclic pitch, and shaft tilt on BMR response and loads. Two of the five blades were extensively instrumented with flatwise and chordwise strain gages. This provided a rare opportunity to validate the state-of-the-art in BMR load prediction capability.

The Sikorsky KTRAN analysis and the Sikorsky version of the University of Maryland Advanced Rotorcraft Code (UMARC/S) were used for the bending moment correlations. These two codes have been used very successfully at Sikorsky for

Presented at the AHS Aeromechanics Specialists Conference, San Francisco, CA, January 19-21, 1994.

predicting the rotor frequency, response and stability of this BMR (Refs. 1-3).

Description of the Experiment

The full-scale rotor experiment was performed at the NASA Ames 40- by 80-Foot Wind Tunnel. A schematic of the rotor is shown in Fig. 1. The rotor was mounted on NASA's Rotor Test Apparatus (RTA). The RTA fuselage was mounted on three struts, which placed the rotor plane 21.5 feet above the tunnel floor. Inside the RTA fuselage were two 1500 hp electric drive motors, a hydraulic actuator system, and a five-component balance that measured three forces and pitching and rolling moments. The entire RTA fuselage could be tilted forward or aft to change the rotor shaft angle.

The rotor system was instrumented with strain gages on the blades (including the flexbeams and torque tubes), the rotating and non-rotating scissors, the rotating and non-rotating pushrods, and the rotor shaft. Each of the five blades was instrumented at the flexbeam root to measure flatwise and chordwise responses. Two of the five blades were extensively instrumented, with strain gages at twelve spanwise locations. Each of these twelve stations included a full-bridged flatwise and chordwise gage to measure the bending moments perpendicular and parallel to the local airfoil axis system. Unfortunately, the number of rotating system measurements was limited by slip ring size. This resulted in having only 5-7 bending moment gages active in each direction at any one time. The radial locations of the bending moment measurements used in this study are listed in Table 1.

Experimental data were obtained over a wide range of test conditions and included the following parametric sweeps:

- Hover collective pitch sweep, θ_{75} from 0.7 deg to 11.7 deg, in 1 deg increments.
- Hover rotor speed sweep from 283 to 346 rpm.
- Forward flight speed sweep at 10,500 lb from 0 to 200 knots.
- Forward flight speed sweep at 14,000 lb from 0 to 160 knots.
- Forward flight speed sweep at 16,000 lb from 0 to 140 knots.
- Thrust sweep at 80 knots from -4,000 to 15,500 lb.
- Thrust sweep at 120 knots from -1,835 to 15,700 lb.
- Shaft angle sweep at 80 knots from +5 deg nose up to -10 deg nose down.
- Rotor speed sweep at 40, 60, 120 and 160 knots, from 255 to 330 rpm.
- Rotor head moment sweep from -15,000 to +15,000 ft- lb in pitch and roll.

Blade bending moment data from the forward flight speed sweep at 14,000 lb thrust were used for the correlation study in this paper. For this sweep, the rotor speed was set to 315 RPM and the rotor was trimmed to representative aircraft steady operating conditions, including shaft angle and rotor hub moments. Data were acquired at a rate of 64 samples/revolution.

Analytical Methodologies

Bearingless rotors have become popular among designers because of a lower parts count, reduced weight, reduced maintenance, suitability to aeroelastic tailoring, improved handling qualities, and extended fatigue life. Concurrently, the analysts are still improving their BMR modeling tools. There have been many studies of the bending loads for articulated rotors, for example Ref. 4. Due to a lack of available data and analytical tools, however, only limited analytical work has been done to correlate the response of bearingless rotors.

The analysis of a bearingless rotor system is more difficult than that of a hingeless or articulated rotor system because of nonlinear structural couplings, snubber/damper assemblies, and redundant load paths. In a bearingless rotor the flap and lag hinges, as well as the pitch bearings, have all been replaced by a torsionally soft flexbeam between the blade and the hub (Fig. 1). Pitch control is applied to the blade by rotating the torsionally stiff torque tube with a pushrod. The torque tube in turn twists the flexbeam. This design results in significant bending-torsion coupling, and requires careful modeling for accurate predictions.

Most modern bearingless rotors, including this Sikorsky 5-bladed BMR, employ a snubber/damper at the inboard end of the torque

tube (Fig. 1). The snubber/damper serves many purposes: the snubber portion provides a pivoting point for the inboard end of the torque tube and prevents excessive static droop, the damper portion functions as a lead-lag damper and introduces positive pitch-lag coupling (lag-back nose-up) to increase lag mode aerodynamic damping. Accurate predictions of blade response and rotor stability require this snubber/damper to be properly modeled.

For bearingless rotors, the blade loads are transferred to the helicopter through the flexbeam, as well as through the torque tube and pushrod. For BMRs that incorporate snubber/dampers, shear loads can transfer between the torque tube and the flexbeam at the snubber junction. These redundant load paths complicate the assembly of blade equations and modeling of the boundary conditions.

In addition to modeling the BMR-specific items mentioned above, a good analysis must account for the coupling between the aeroelastic problem and the trim state of the helicopter. This requires that the nonlinear blade response and nonlinear trim equations be solved together.

Two computer programs were employed for the correlation described in this paper. They are the Sikorsky KTRAN analysis and the Sikorsky version of UMARC. A brief description of each program follows.

KTRAN

KTRAN was developed at Sikorsky Aircraft for the prediction of rotor loads and response. The analysis includes coupled elastic flap, lag and torsion degrees of freedom. Fuselage dynamics are not included. The blade equations of motion are solved using the finite segment transfer matrix method. The bearingless rotor is modeled as a multiple load path system with up to fifty discrete elements for the blade and flexbeam, and up to twenty elements for the torque tube. For the analysis of this S-76 BMR, thirty elements are used for the blade, twenty for the flexbeam and twenty for the torque tube.

Control system stiffness is modeled with a torsion spring connected between the ground and the torque tube. The snubber/damper is modeled as a spring and damper system linked between the torque tube and the flexbeam. The spring/damper model rotates with the torque tube.

Blade element theory and airfoil table lookup are used for aerodynamic calculations. Free wake modeling is used for enhancing the prediction of higher harmonic aerodynamic forces. The UTRC Freewake analysis has two options: a distorted wake and a classical wake. The blade response is assumed to be a sum of many harmonics. The responses to each harmonic airload are calculated and then added together. The blade response is iterated until it reaches a steady state. The analysis can be trimmed to converge on prescribed rotor thrust and rotor moments, or to prescribed control settings.

Unlike most finite element analyses, the transfer matrix method requires a compatibility of the displacement and slope, as well as the forces and moments between elements. The benefit of the transfer matrix method is that the shear forces and bending moments are known immediately when the response is solved. In KTRAN, the forces and moments are calculated at the middle of each element.

A second advantage of the transfer matrix method is its speed. The matrix size for the blade equation is always the same as the number of state variables used for each element; it is independent of the number of elements used. The KTRAN modeling of the BMR is shown in Fig. 2. There are 10 states at each end of the element. The displacements and slopes are x = [v, v', w, w' ϕ], and the forces and moments are F = [Fy, Mz, Fz, My, Mx]. For example, the displacements and forces at the left and right ends of element number one are related by a 10x10 transfer matrix T_{21}.

$$\begin{Bmatrix} x \\ F \end{Bmatrix}_2 = \left[T_{21} \right] \begin{Bmatrix} x \\ F \end{Bmatrix}_1$$

If n number of elements are used, then the blade equation simply becomes:

$$\begin{Bmatrix} x \\ F \end{Bmatrix}_n = \left[T_{(n,n-1)}\right] \cdots \left[T_{21}\right] \begin{Bmatrix} x \\ F \end{Bmatrix}_1$$

$$= \left[T_{n1}\right] \begin{Bmatrix} x \\ F \end{Bmatrix}_1$$

The drawback of the transfer matrix method is that if a new load path is added to the rotor, the above equation must be rewritten to satisfy the compatibility at the junction.

UMARC/S

The University of Maryland's UMARC analysis (Refs. 5-6) has been modified at Sikorsky to analyze the S-76 BMR with a snubber/damper. A modal and a force summation method have also been added to calculate the BMR bending moments. UMARC is based on a finite element method in space and time. The hub motions are not included in the response calculations. The blade is assumed to be an elastic beam undergoing flatwise bending, chordwise bending, elastic twist and axial extension. This Bernoulli-Euler beam is allowed small strains and moderate deflections. Due to the moderate deflection assumption, the equations contain nonlinear structural, inertial and aerodynamic terms. The blade can be discretized into a number of beam elements. For this BMR, five elements are used for modeling the blade, six for the flexbeam, and five for the torque tube. Each element has fifteen degrees of freedom (Fig. 3). Between elements there is a continuity of displacement and slope. The snubber/damper is modeled as a spring and damper system linked between the flexbeam and the torque tube. The spring/damper system rotates with the torque tube when blade pitch is changed. The aerodynamic modeling includes quasi-steady strip theory, the Leishman and Beddoes 2-D unsteady aerodynamic model for capturing the unsteady shed wake, trailing edge separation and dynamic stall, and a Scully free wake to capture the 3-D trailed wake and higher harmonic forcing.

Results from UMARC include blade displacement and slope. Additional work must be done to obtain the bending moments. Two methods have been added to UMARC/S to calculate the bending moments. The modal method uses the flatwise and chordwise stiffness (EI_y and EI_z) and the second derivatives (w" and v") calculated at the finite element Gaussian integration points to get the bending moments. The force summation method sums up the aerodynamic and inertial loads from the necessary elements to obtain the bending moment at the inboard end of each element.

Using $EI_y w''$ and $EI_z v''$ to obtain the bending moment is straightforward. The advantage is once the response has been solved, the slopes w" and v" are known everywhere on the blade, flexbeam and torque tube. This method is independent of rotor type (articulated, hingeless or bearingless). The primary drawback is that accurate results require the use of either 1) many elements, or 2) elements with non-uniform stiffness.

Sixteen elements are sufficient for predicting the rotor response and stability of this BMR (Ref. 2). However, the stiffness inside each element is assumed constant, and the value represents an average stiffness in that region. Some inaccuracy arises when extracting "local" information, such as the local bending moment at the flexbeam root.

The force summation method is straight forward to implement for an articulated or hingeless rotor, but becomes quite involved for a BMR. To obtain the bending moment in the blade, the procedure simply requires summing up the loads from the "outboard" elements. This is identical to solving for the moments for articulated and hingeless blades. However, to find the moments for the flexbeam or the torque tube, the loads from the "redundant" path must be subtracted from the loads from the blade portion.

For example, to find the moment on the flexbeam, the shear forces and bending moments at the flexbeam/blade/torque tube junction that are fed back from the torque tube must be accounted for. These extra forces and moments are due to the aerodynamic and inertial forces acting on the torque tube, the internal bending moment of the torque tube itself, the reaction force from the pushrod and the reaction force at the snubber/damper. The most demanding part is calculating a precise displacement for the torque tube at the pushrod location, and a precise relative displacement between the torque tube and the flexbeam at the snubber. The flatwise

bending moment in the flexbeam is very sensitive to these two reaction forces. Fig. 4 illustrates the forces and moments involved in using a force summation method to obtain the flatwise bending moment at a location "x" in the flexbeam.

Analytical Approach

For the results presented in this paper, both the KTRAN and UMARC/S prediction methods were set to converge on the rotor thrust and pitching moments measured by the RTA balance. Predictions were made both with and without a free wake model. All UMARC/S calculations included the Leishman and Beddoes 2-D unsteady aerodynamic model.

The radial stations at which the bending moments were calculated were chosen to match the actual measurement locations whenever practical. Because of modeling differences in the prediction methods, however, exact matches were not always obtained. The increment in azimuthal position was different for each method; the KTRAN results were calculated every 12 deg in azimuth, while the UMARC/S results were calculated every 18 deg. This compares with the test data increment of 5.625 deg.

Results and Discussion

This section presents the correlation results for each of the prediction methods, along with some limited discussion. Included in these results are 3-D contour plots, which allow qualitative assessments of bending moment waveforms, and harmonic plots, which allow quantitative assessments. In addition to these results, a number of items are presented which may prove useful in future correlation efforts. These include the effect of various parameters on predictions, and a discussion of the limitations of the force summation method.

Bending Moment Waveforms

Figures 5-9 present measured and predicted bending moment time histories using a 3-D contour plot format. This format allows a qualitative assessment of how well the bending moment waveform is predicted. The results in these figures are for forward speeds from 40 to 150 knots, at a constant 14,000 lb thrust. The predictions include harmonic response from the 0 to 8th harmonic. The test data are "smoothed" time histories, averaged over 8 revolutions with all non-harmonics removed. The bending moments are plotted against blade span and azimuth for one rotor revolution and include both steady and vibratory components. Note that the bending moments in these and all other figures in this paper have been non-dimensionalized. For purposes of comparing the relative waveforms, the predicted data have been shifted in azimuth to best match the measured data.

Figures 5 and 6 present the measured and KTRAN-predicted flatwise and chordwise bending moments for forward speeds from 40 to 150 knots. The KTRAN predictions utilized a distorted free wake model. In general, the predicted waveforms match the test data reasonably well for all speeds and all gage locations. In addition, the moment amplitudes are fairly well predicted, with slightly worse correlation near the flexbeam/blade junction ($x/R = 0.26$). These results are especially encouraging for the chordwise bending moments since they have traditionally been much more difficult to predict than flatwise moments.

The effect of not including the free wake in the KTRAN predictions is shown in Fig. 7. This figure shows both the measured and predicted flatwise and chordwise moments at 80 knots. As expected, the predictions show much less higher harmonic content, especially near the flexbeam/blade junction, than either the test data or predictions with the free wake (see Fig. 5d and 6d).

Figures 8 and 9 compare the measured data at one forward speed (100 knots) with predictions from all three analytical methods: the KTRAN matrix approach (with free wake), the UMARC/S modal approach (with and without the Scully free wake), and the UMARC/S force summation approach (without free wake). For the flatwise bending case (Fig. 8), the magnitude and waveform are predicted well by all except the force summation method. For the chordwise case (Fig. 9), all methods predict the waveform well, but the UMARC/S methods tend to overpredict the magnitude near the flexbeam root. For both cases, the inclusion of a free wake model in the

UMARC/S predictions increases the higher harmonic content on the blade and near the flexbeam/blade junction.

The results of Figs. 8 and 9 are typical of those at other speeds. In particular, the moment waveforms are predicted reasonably well by both KTRAN and the UMARC/S modal method, but not by the force summation method. The reasons for the poor correlation with this latter method will be discussed later in the paper.

As mentioned earlier, the predicted data in Figs. 5-9 were shifted in azimuth to match the measured data and allow easier comparisons of the bending moment waveforms. The flatwise predictions required about a 15 deg azimuth shift. One possible explanation for this phase shift is that incorrect values of rotor hub pitching and rolling moment were input to the analyses. This is possible since the inputs came from RTA balance measurements. These measurements included not only the true rotor hub moments, but also the loads through the redundant load path (torque tube/pushrod).

The chordwise correlation shows a larger azimuth shift, on the order of 60 deg. The reason for this shift is unknown. One of the possibilities is that the true lead-lag motions are highly coupled with the transmission/drive system. For example, Ref. 2 showed the collective lag frequency for this rotor is reduced from 3.7 to 2.5 Hz due to a coupling with the transmission. This coupling effect is not modeled in the analyses.

Bending Moment Harmonics

Figures 10 and 11 present both measured and predicted harmonic bending moment information (including magnitude and phase) for one forward speed (100 knots). These figures allow a more quantitative assessment of the bending moment predictions than the previous 3-D contour figures. The predictions were done using KTRAN (with free wake) and the UMARC/S modal approach (with and without free wake). The force summation results are not included, since their qualitative chordwise results were poor.

Flatwise Harmonics-Magnitude (Fig. 10a)

The magnitudes of the flatwise bending moments for the 0-6P harmonics are shown in Fig. 10a. All three prediction methods match the test data fairly well, with the largest discrepancies near x/R=0.3.

The effect of a free wake model can be seen at the higher harmonics, especially at 3, 4, and 5P. The KTRAN and UMARC/S predictions that include a free wake model show greater amplitude (and better correlation) for the higher harmonics than those predicted by UMARC/S without a free wake. As expected, UMARC/S shows the free wake makes little difference on the 0-th and 1P harmonics.

Flatwise Harmonics-Phase (Fig. 10b)

The phases of the flatwise bending moments for the 0-6P harmonics are shown in Fig. 10b. All three prediction methods correlate the first harmonic phase to within 15 deg. This is the same amount of azimuth shift necessary to improve the 3-D contour correlation in Fig. 5. Significant phase differences show up at the higher harmonics, although the curve shapes of the predictions match the test data fairly well.

It is expected that inclusion of a 2-D unsteady aerodynamic model (as in UMARC/S) will improve the prediction of bending moment phase. In particular, the model can account for the delay in the lift build-up due to a change in blade response. Unfortunately, the results of this study are inconclusive, since 1) no UMARC/S predictions were performed without the aerodynamic model and 2) the UMARC/S predictions show no significant improvement over the KTRAN results.

Chordwise Harmonics-Magnitude (Fig. 11a)

The magnitudes of the chordwise bending moment harmonics are shown in Fig. 11a. In general, the curve shapes of the predictions match the test data fairly well (also seen in Fig. 6). The magnitudes, however, are not as well predicted, especially near the flexbeam root. For example, all the analyses overpredict the moments on the blade for 1P-3P and at the flexbeam root for 2P.

The inclusion of a free wake model in UMARC/S shows little effect on the 0-th and 1P harmonic predictions. At higher frequencies, UMARC/S with the free wake model generally predicts higher moments than UMARC/S without, especially on the flexbeam. Correlation with test data, however, is not necessarily improved by inclusion of the model.

Chordwise Harmonics-Phase (Fig. 11b)

The phases of the chordwise bending moment harmonics are shown in Fig. 11b. None of the analyses match the phase amplitude accurately, although the curve shapes of the predictions match the test data fairly well at some of the harmonics.

Physical Understanding of Harmonic Plots

This section attempts to provide a physical understanding of the harmonic plots in the previous section. In particular, the relationship between the phase plots and the blade modes are discussed.

Figures 12 and 13 present the Southwell diagrams for this S-76 BMR as predicted by KTRAN and UMARC/S, respectively. Excellent frequency correlation with the data is obtained for both analyses. This yields confidence in the structural properties used as input to the dynamics calculations, and provides a basis for the following discussion.

For the nominal operating rotor speed of 315 rpm, Figs. 12 and 13 show that only the first flap and first lag modes are in the region near 1P. Therefore, the 1P flatwise and 1P chordwise bending moments are due primarily to the 1F and 1L motion of the blade. Thus, the 1P phase plots in Figs. 10b and 11b are related to first elastic bending modes.

The second flap mode frequency is between the 2P and 3P excitation frequencies. Hence, in Fig. 10b, the phase plot for the 2P and 3P flatwise bending moment is related to a second elastic bending mode. Since there are no lag modes near 2P and 3P, the phase plots for 2P and 3P chordwise moments in Fig. 11b are relatively flat. When there isn't a structural mode near the harmonic excitation, the structural response is weak and it becomes difficult for the analyses to predict either the phase or the magnitude. Figure 11b shows the 2P and 3P phase predictions are very poor for both analyses. Figure 11a also shows that the 2P and 3P chordwise magnitudes are over-predicted.

The third flap frequency is between 4P and 5P. Hence, in Fig. 10b, the phase plots for the 4P and 5P flatwise bending moments are related to a third elastic bending mode. The second lag mode is also between 4P and 5P. Thus, the 4P and 5P chordwise phase plots (Fig. 11b) should be related to the second lag mode. The relationship with the 5P phase is not clear, however, since the 2L and 3F modes are highly coupled near 5P.

Miscellaneous Results

During the course of this correlation effort, many things were learned which may be of benefit in future studies. Some of these are presented in this section. In particular, the effect of analysis approach on blade tip response, the effect of various parameters on steady chordwise moment predictions, and a discussion of the limitations of the force summation method are presented.

Blade Tip Response

Figures 14 and 15 compare the predicted blade tip response from KTRAN and UMARC/S for the 100 knot case. The flap responses match well. The lead-lag responses show a phase difference and a magnitude difference. The phase difference can probably be attributed to the different aerodynamic models used, with the 2-D unsteady aerodynamics in UMARC/S accounting for a delay in lift buildup. One possibility for the magnitude difference is the different structural modeling of the blade torque offset and neutral axis.

Parameter Effects on Steady Chordwise Moments

Figures 16 and 17 demonstrate the importance of neutral axis and torque offset modeling on steady chordwise bending moment predictions. Torque offset is used in BMR designs to minimize the steady lag angle (similar to the way precone minimizes the steady flap angle). For this rotor, it is a 1-inch forward offset, from the axis of

rotation, of the elastic axis at the flexbeam-to-rotor-hub junction.

Figure 16 shows the effect of neutral axis placement on steady bending moment predictions for a 14,000 lb thrust, 80 knot condition. The results, calculated using KTRAN, clearly indicate the importance of this parameter for predicting the loads accurately.

Figure 17 shows the effect of torque offset modeling on the predicted chordwise bending moment in hover. For illustration purposes, calculations were done with zero precone at C_T/σ = .001. The results were calculated using the modal method and the force summation method in UMARC/S. The modal method already includes the torque offset effect in the calculated lead-lag displacement and second derivative (v and v''). In the force summation method, the tangential component of the centrifugal load has to be added in addition to the aerodynamic and inertial load. Otherwise, the blade lags excessively as shown in Fig. 17.

Figure 18 demonstrates the importance of properly treating the loads feeding back from the redundant load path when using the force summation method. For illustration purposes, calculations were done with zero precone and zero torque offset at C_T/σ = .001. Neglecting the redundant load path gives incorrect results for the steady flexbeam chordwise-bending moment. Note that the difference in the bending moments for the blade is not related to the redundant load path but rather is due to differences between the modal and force summation methods.

Limitations of Force Summation Method

Figures 19a and 19b illustrate the difficulty of using a force summation method to predict the flatwise bending moment in the flexbeam. Figure 19a is for a hover condition at C_T/σ = .001. Figure 19b is for a hover condition at C_T/σ = .093 (14,000 pounds thrust). The flatwise bending moments predicted by the UMARC/S force summation method are compared to the UMARC/S modal method. The bending moment distribution in the blade section matches well between the two methods. However, the comparison in the flexbeam section is poor. The reason is that the moments inside the flexbeam are very sensitive to the vertical shear load feeding back from the pushrod and the snubber.

Figure 4 shows that the reaction force from the pushrod is $K_p \cdot w_p$, and the reaction force from the snubber is $K_s \cdot w_s$. Since the vertical displacements w_p and w_s are very small, on the order of 0.001 to 0.03 in (depending on thrust), any small inaccuracy in the predicted w displacements may cause significant error when multiplied by a large value for the spring stiffness. Figure 19 shows that if the vertical displacements are arbitrarily reduced by a factor, then the prediction for the flexbeam improves. Figures 19a and 19b show that different correction factors are needed for the zero thrust and 14,000 pounds thrust condition. In Fig. 8e, the flatwise bending moments obtained from the force summation method are uncorrected, hence, significantly different from the others.

The same problem does not exist for the prediction of chordwise bending moments (Fig. 9e) because the snubber has a very weak spring force in the chordwise direction, and the pushrod has no spring restraint for inplane motion.

Conclusions

A study was undertaken to compare measured and predicted flatwise and chordwise bending moments for a full-scale bearingless main rotor. The overall agreement between the measured data and the predictions helps validate the structural inputs and two of the BMR analyses used at Sikorsky: the KTRAN transfer matrix method and the UMARC/S modal method. The following specific conclusions can be drawn from this study:

1) Correlation of KTRAN and UMARC/S predicted blade frequencies with test data is excellent. This validates the structural inputs to the analyses.

2) Both the KTRAN transfer matrix method and the UMARC/S modal method provide good qualitative predictions of blade bending moment waveforms. The primary advantage of the

transfer matrix method is its calculation speed while the primary advantage of the modal method is its ease of implementation.

3) The UMARC/S force summation method is awkward for a BMR with multiple load paths. It does yield good results for chordwise bending moment predictions but not for flatwise predictions.

4) The transfer matrix and modal methods both predict the 0-6P flatwise-bending harmonic magnitudes fairly well. The harmonic phase predictions are not as accurate, although the curve shapes of the predictions match the test data.

5) The transfer matrix and modal methods both predict the curve shape of the chordwise-bending harmonic magnitudes very well. The magnitudes, however, are not as well predicted, especially near the flexbeam root. Neither of the analyses match the phase amplitude accurately, although the curve shapes of the predictions match the test data at some of the harmonics.

6) Using a free wake model improves the prediction of the higher harmonic magnitudes of the flatwise bending moments.

7) A precise knowledge of the blade neutral axis location and torque offset is important for predicting the steady portion of the chordwise bending moment.

Acknowledgement

The authors gratefully acknowledge help from Kurt Hilzinger for running the KTRAN cases, and the insightful discussions with Wen-Liu Miao, Tim Krauss, Bob Blackwell, Mike Torok, Shyi-Yaung Chen, and Jim Duh of Sikorsky Aircraft, and Gunjit Bir and Senthilvel Vellaichamy of the University of Maryland.

References

1. Norman, T. R., Cooper, C. R., Fredrickson, C. A., and Herter, J. R., "Full-scale Wind Tunnel Evaluation of the Sikorsky Five-bladed Bearingless Main Rotor," 49th Annual Forum of the American Helicopter Society, St. Louis, Missouri, May 19-21, 1993.

2. Wang, J. M., Duh, J., Fuh, J-S., and Kottapalli, S., "Stability of the Sikorsky S-76 Bearingless Main Rotor," 49th Annual Forum of the American Helicopter Society, St. Louis, MO, May 1993.

3. Tischler, M. B., Driscoll, J., Cauffman, M. G., and Freedman, C. J., "Study of Bearingless Main Rotor Dynamics from Frequency-Response Wind Tunnel Test Data," AHS Aeromechanics Specialists Conference, San Francisco, CA, Jan., 1994.

4. Torok, M. S., and Goodman, R. K., "Analysis of Rotor Blade Dynamics Using Experimental UH-60A Airloads Obtained at the DNW," 47th Annual Forum of the American Helicopter Society, Phoenix AZ, May 1991.

5. Bir, G. S., Chopra, I., and Nguyen, K., "Development of UMARC (University of Maryland Advanced Rotorcraft Code)," 46th Annual Forum of the American Helicopter Society, Washington, D.C., May 1990.

6. "Theory Manual for University of Maryland Advanced Rotorcraft Code," University of Maryland Aerospace Department, College Park, MD, 1993.

Table 1. Bending moment gages used for correlation

	Radial location x/R	Flatwise gage	Chordwise gage
Flexbeam	0.045		X
	0.070	X	
	0.085	X	
	0.095	X	
	0.150		X
	0.222	X	X
Blade	0.314	X	X
	0.500	X	X
	0.600	X	X

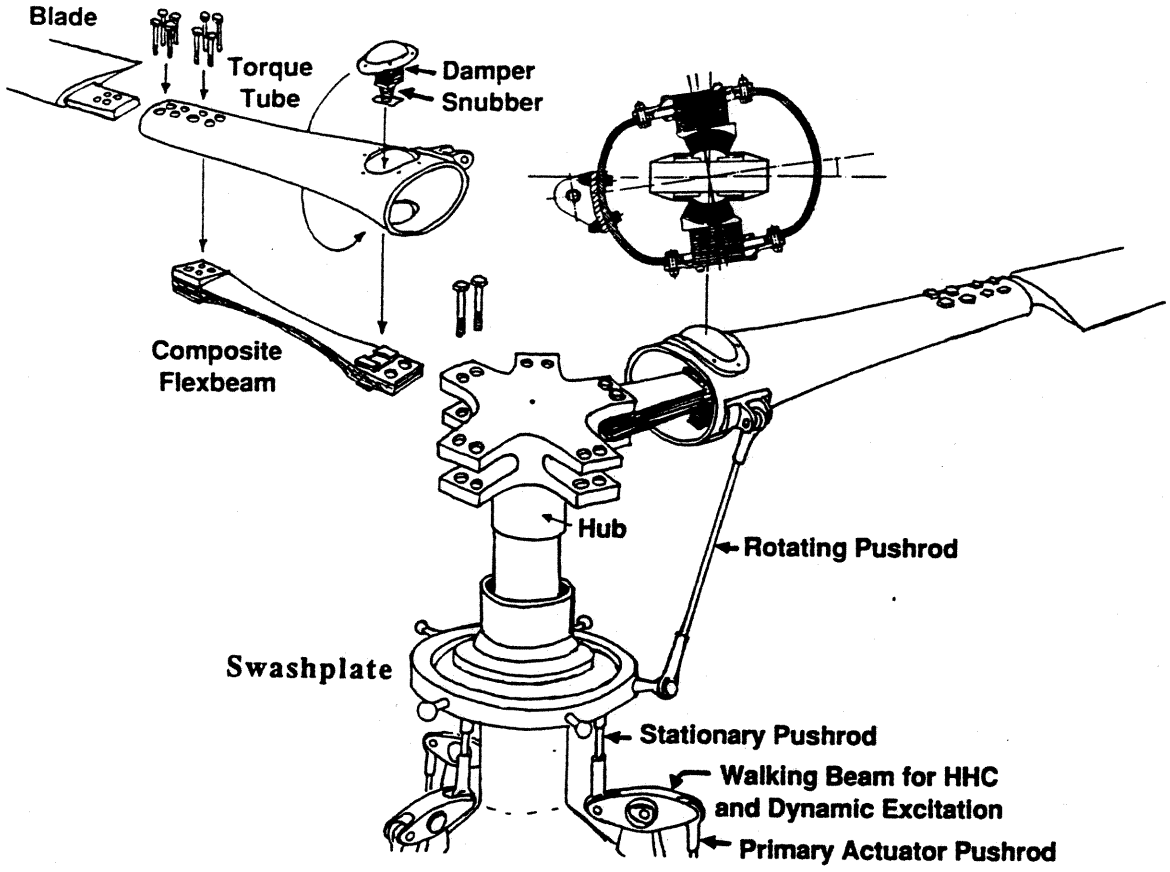

Figure 1. Sikorsky proof-of-concept 5-bladed bearingless main rotor.

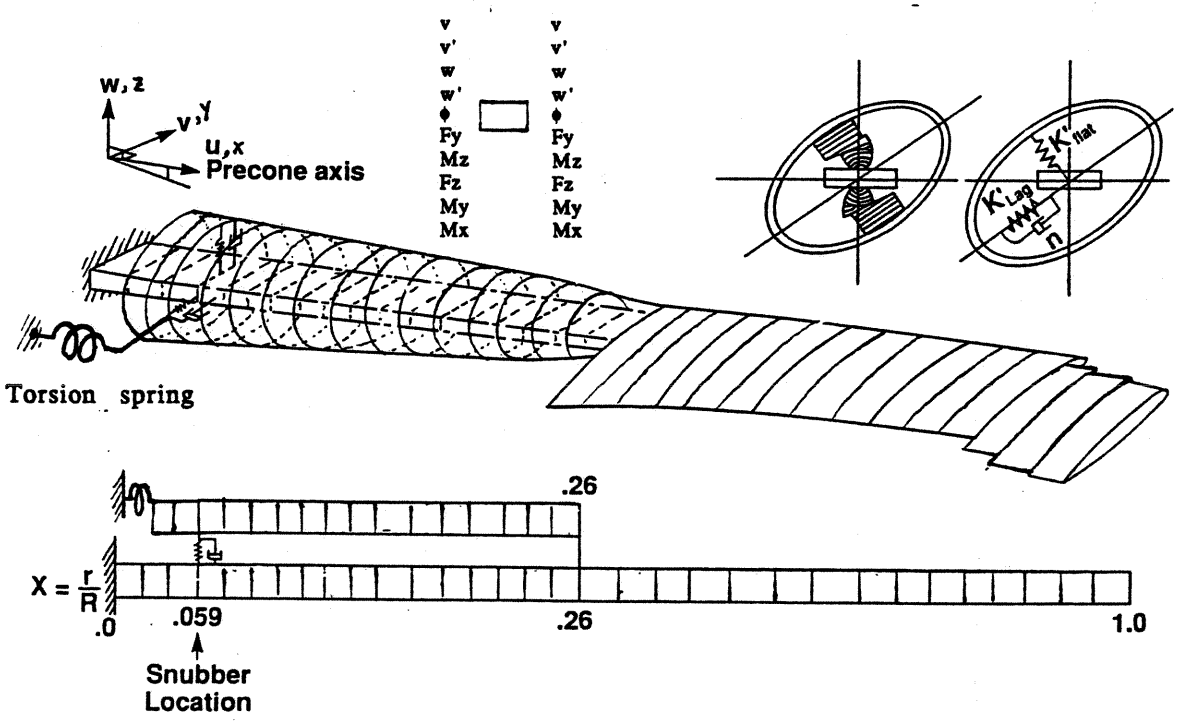

Figure 2. BMR model used in the Sikorsky KTRAN analysis.

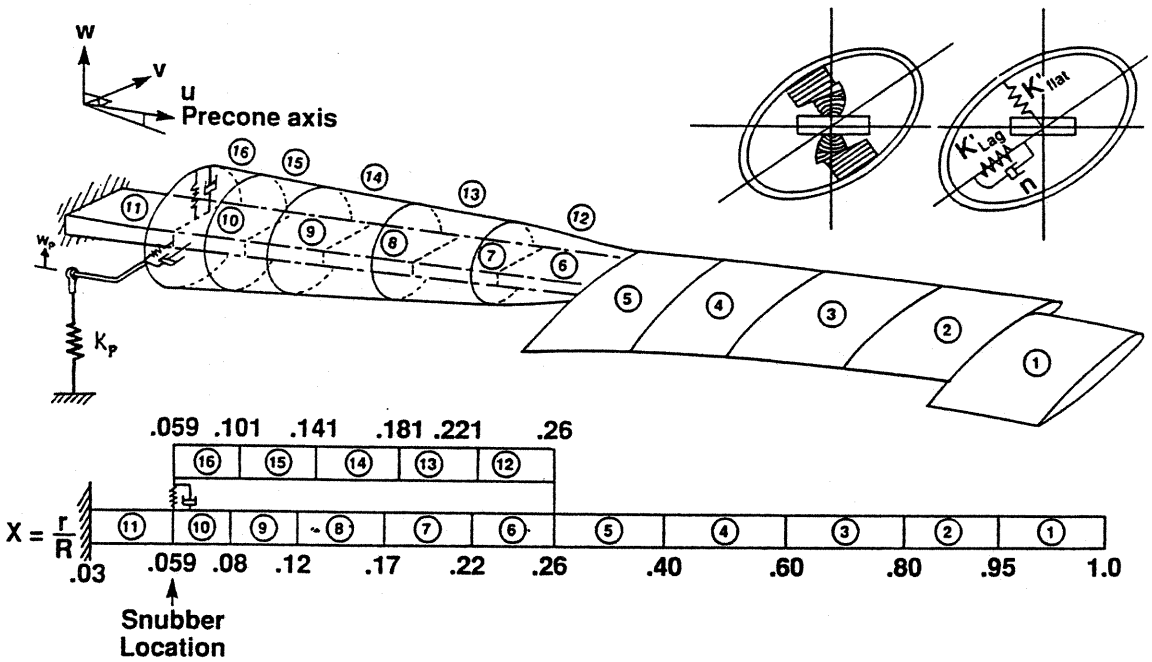

Figure 3. BMR model used in the Sikorsky UMARC/S analysis.

u	u = Axial
v	v = Lead-lag
v'	v' = Slope
w	w = Flap
w'	w' = Slope
ϕ	ϕ = Torsion

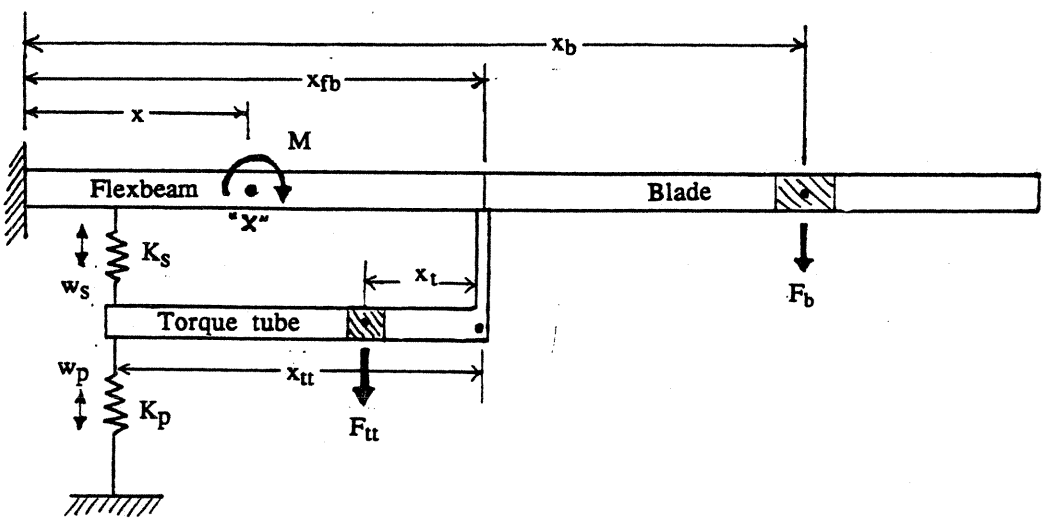

M = moment from blade + moment at "x" due to shear at flexbeam/blade junction + moment at "x" due to moment at junction

M = moment from blade + (tt shear - spr. forces)*arm + (-tt moment + moment from spr.)

$$M = \sum_{b=1}^{n_b} F_b \cdot (x_b - x) + \left(\sum_{tt=1}^{n_{tt}} F_{tt} - (K_p \cdot w_p + K_s \cdot w_s) \right) \cdot (x_{fb} - x) - \sum_{tt=1}^{n_{tt}} F_{tt} \cdot x_t + (K_p \cdot w_p + K_s \cdot w_s) \cdot x_{tt}$$

Figure 4. The forces and moments in the force summation model of a BMR.

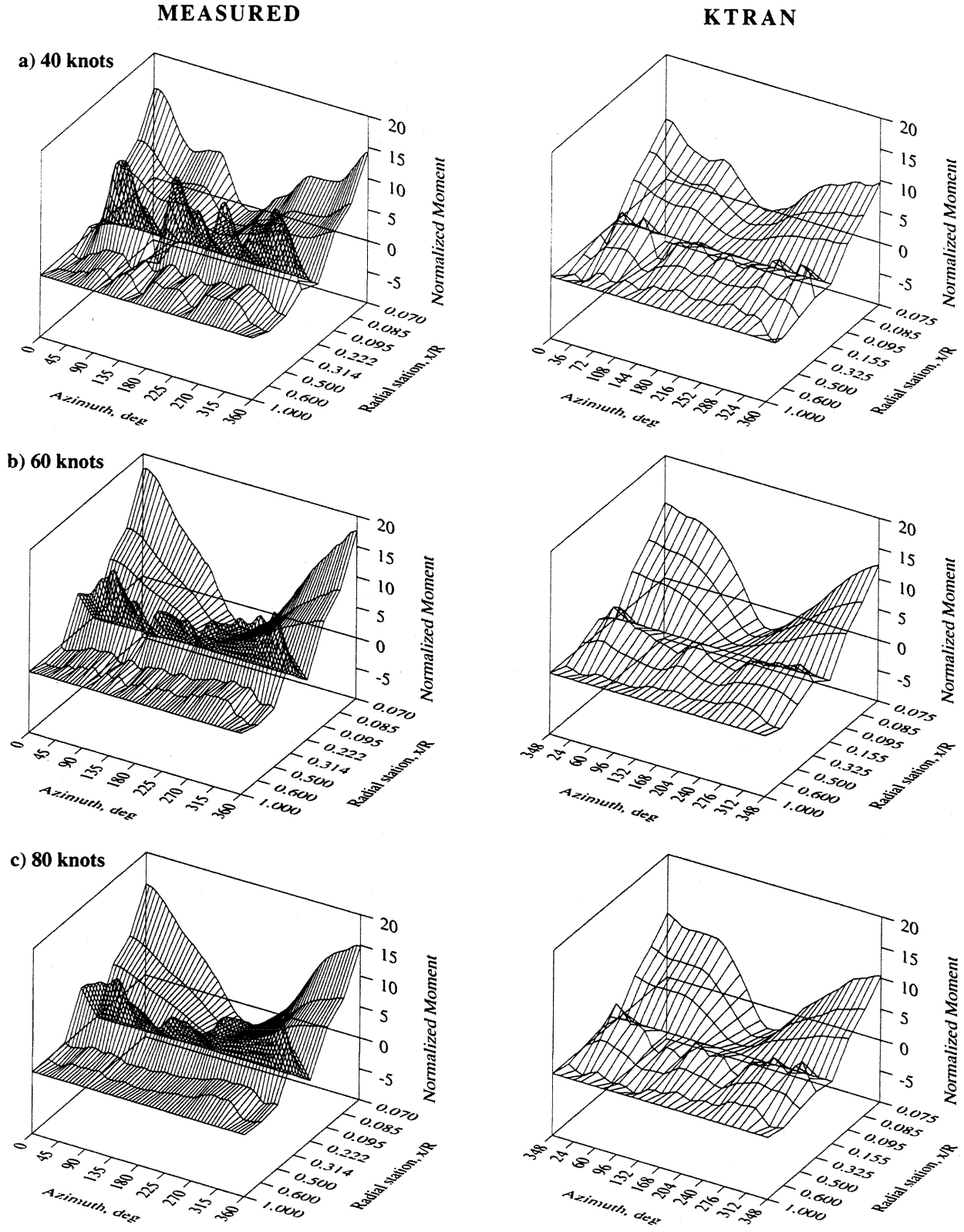

Figure 5. Measured and KTRAN-predicted (with free wake) flatwise bending moments, 14000 lb thrust, 315 RPM, a) 40 knots, b) 60 knots, c) 80 knots.

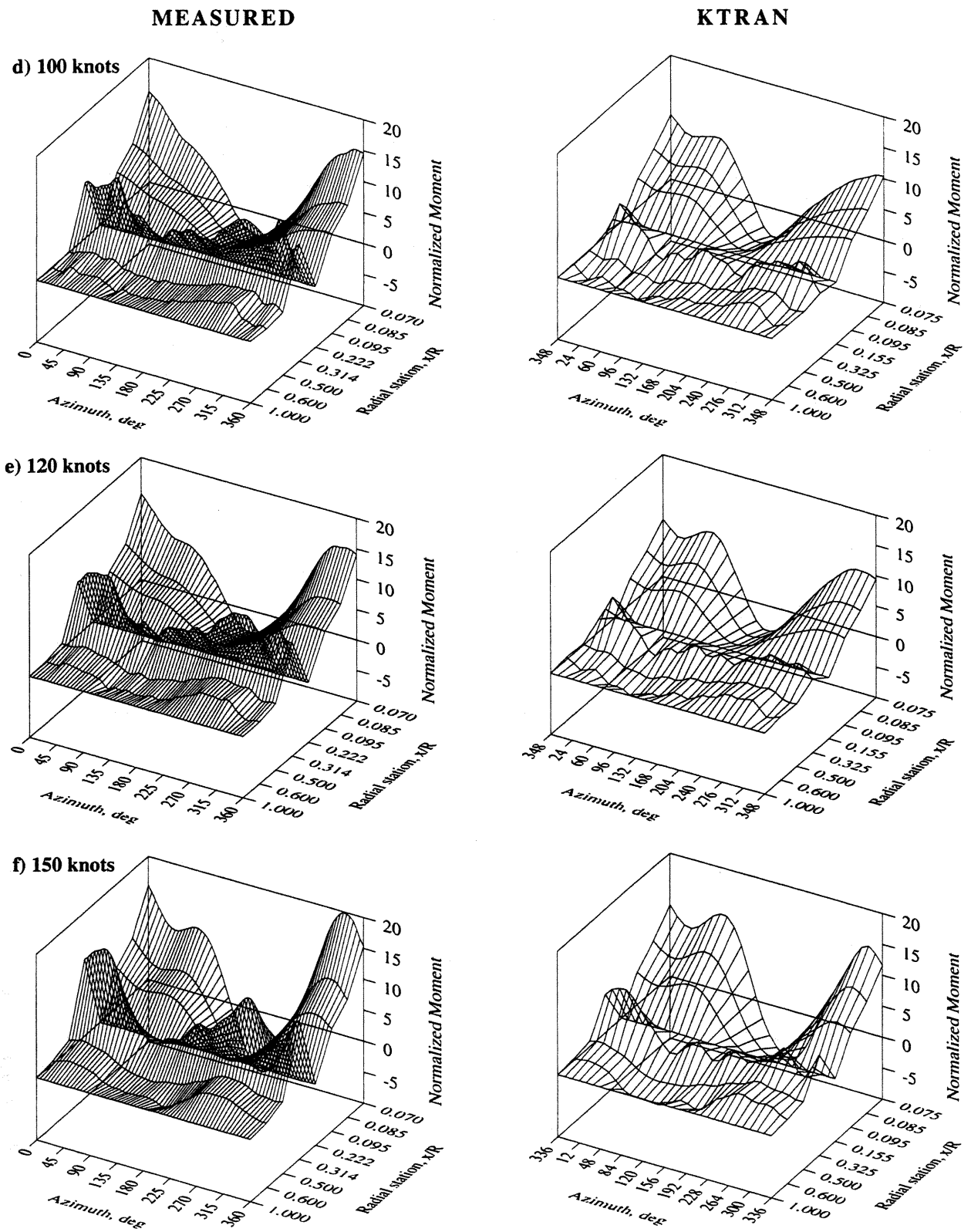

Figure 5. Measured and KTRAN-predicted (with free wake) flatwise bending moments, 14000 lb thrust, 315 RPM, d) 100 knots, e) 120 knots, f) 150 knots.

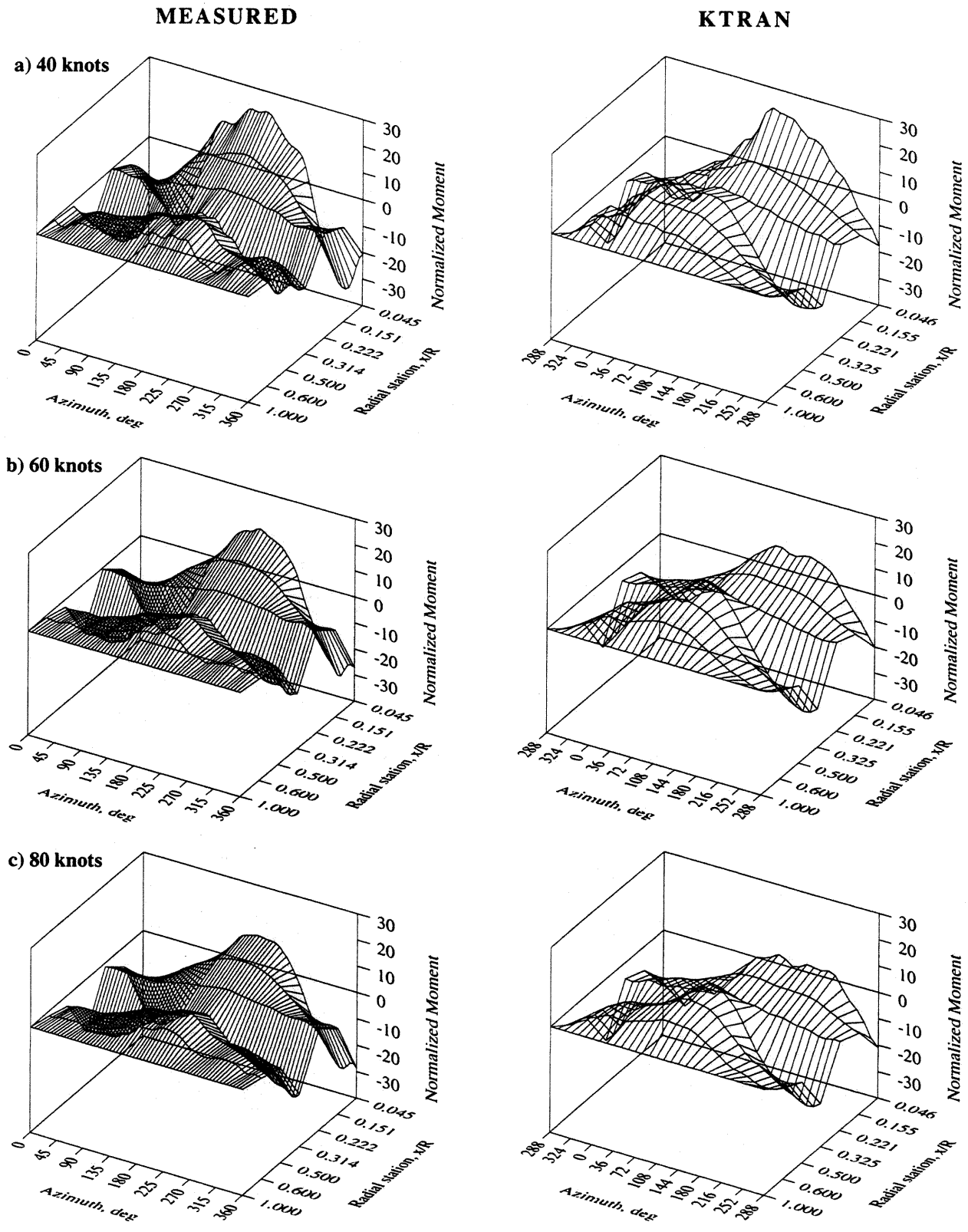

Figure 6. Measured and KTRAN-predicted (with free wake) chordwise bending moments, 14000 lb thrust, 315 RPM, a) 40 knots, b) 60 knots, c) 80 knots.

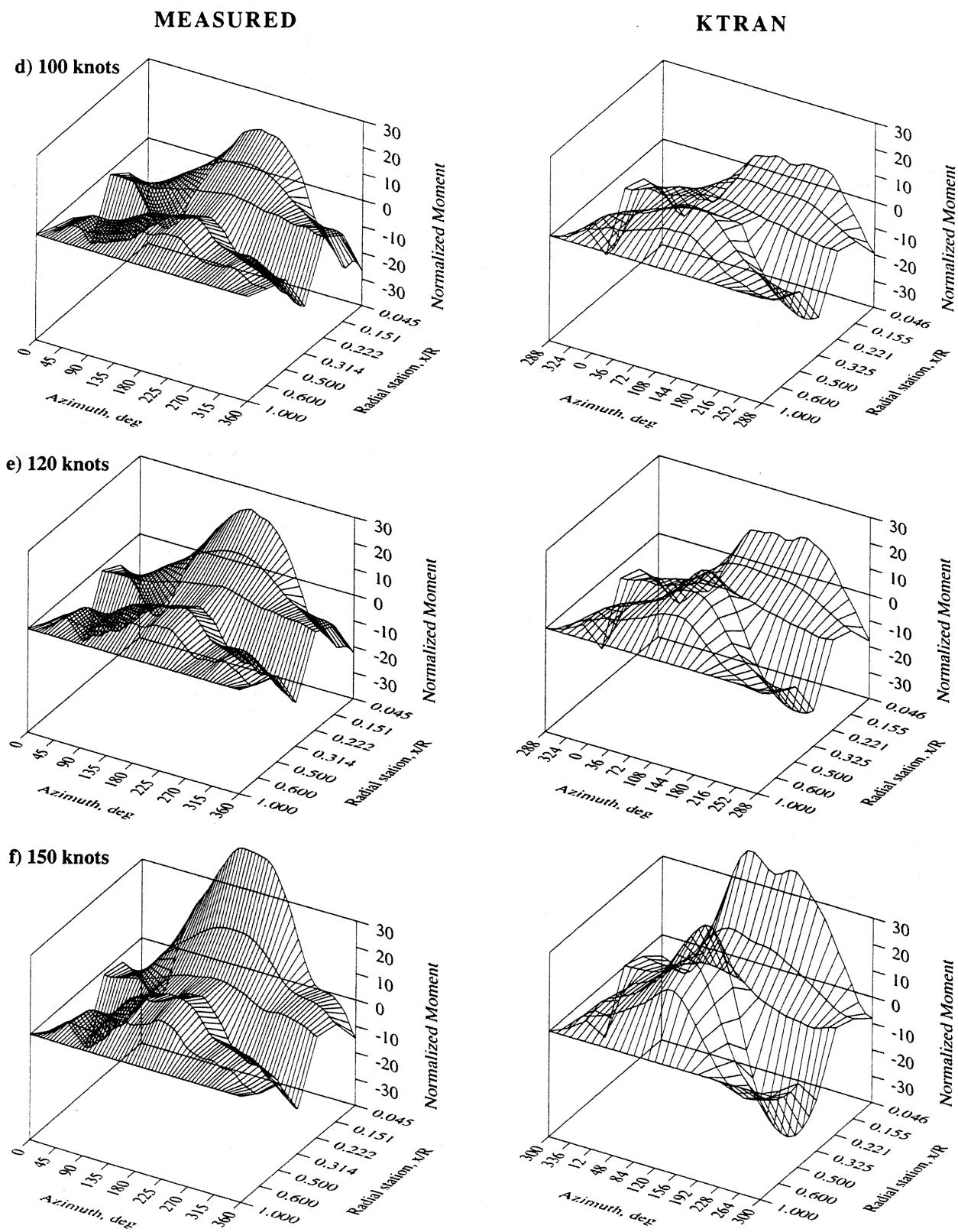

Figure 6. Measured and KTRAN-predicted (with free wake) chordwise bending moments, 14000 lb thrust, 315 RPM, d) 100 knots, e) 120 knots, f) 150 knots.

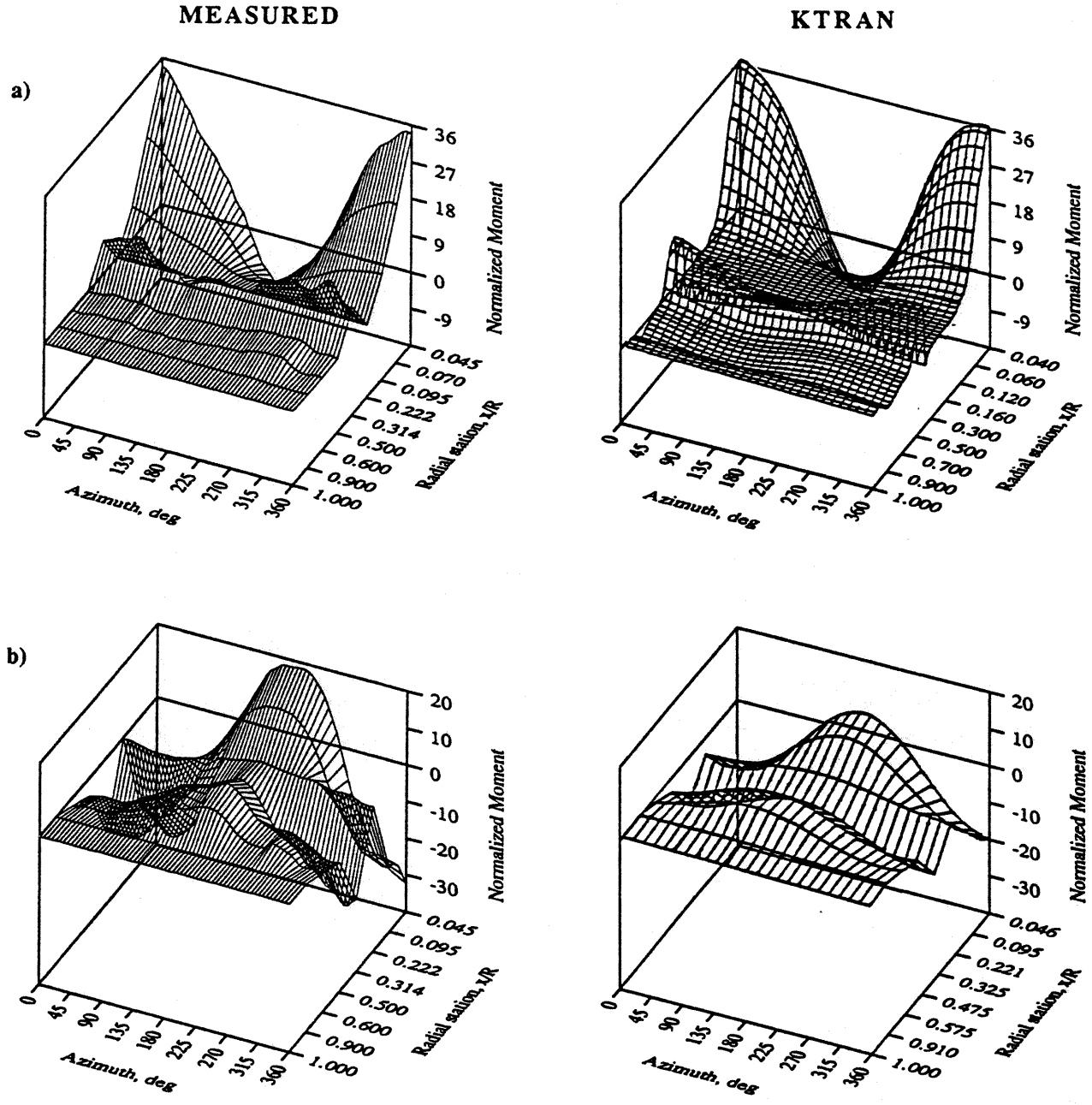

Figure 7. Measured and KTRAN-predicted (without free wake) bending moments, 80 knots, 14000 lb thrust, 315 RPM, a) flatwise, b) chordwise

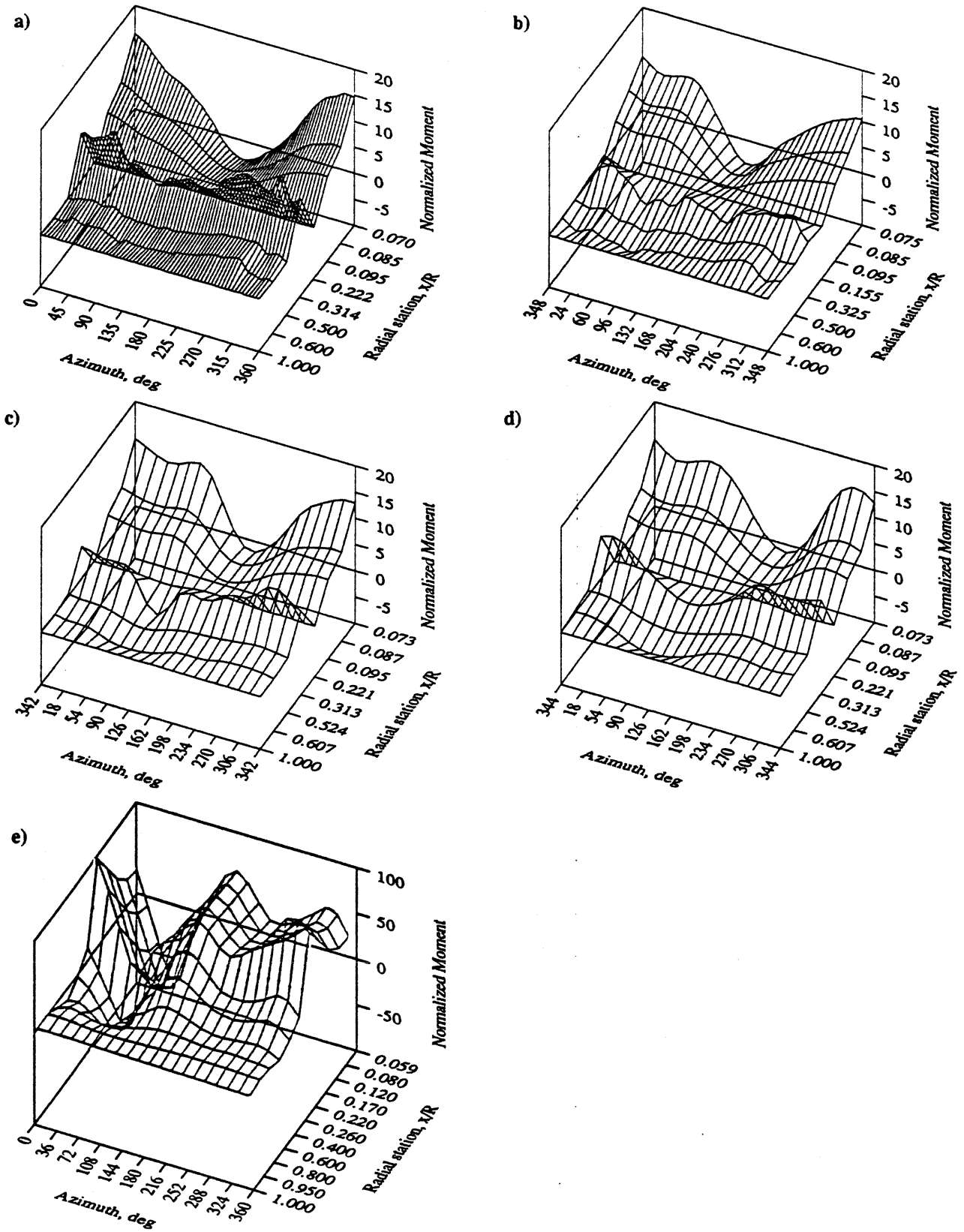

Figure 8. Flatwise bending moment, 100 knots, 14000 lb thrust, 315 RPM, a) measured, b) KTRAN (with free wake), c) UMARC/S modal method (with free wake), d) UMARC/S modal method (without free wake), e) UMARC/S force summation method (without free wake).

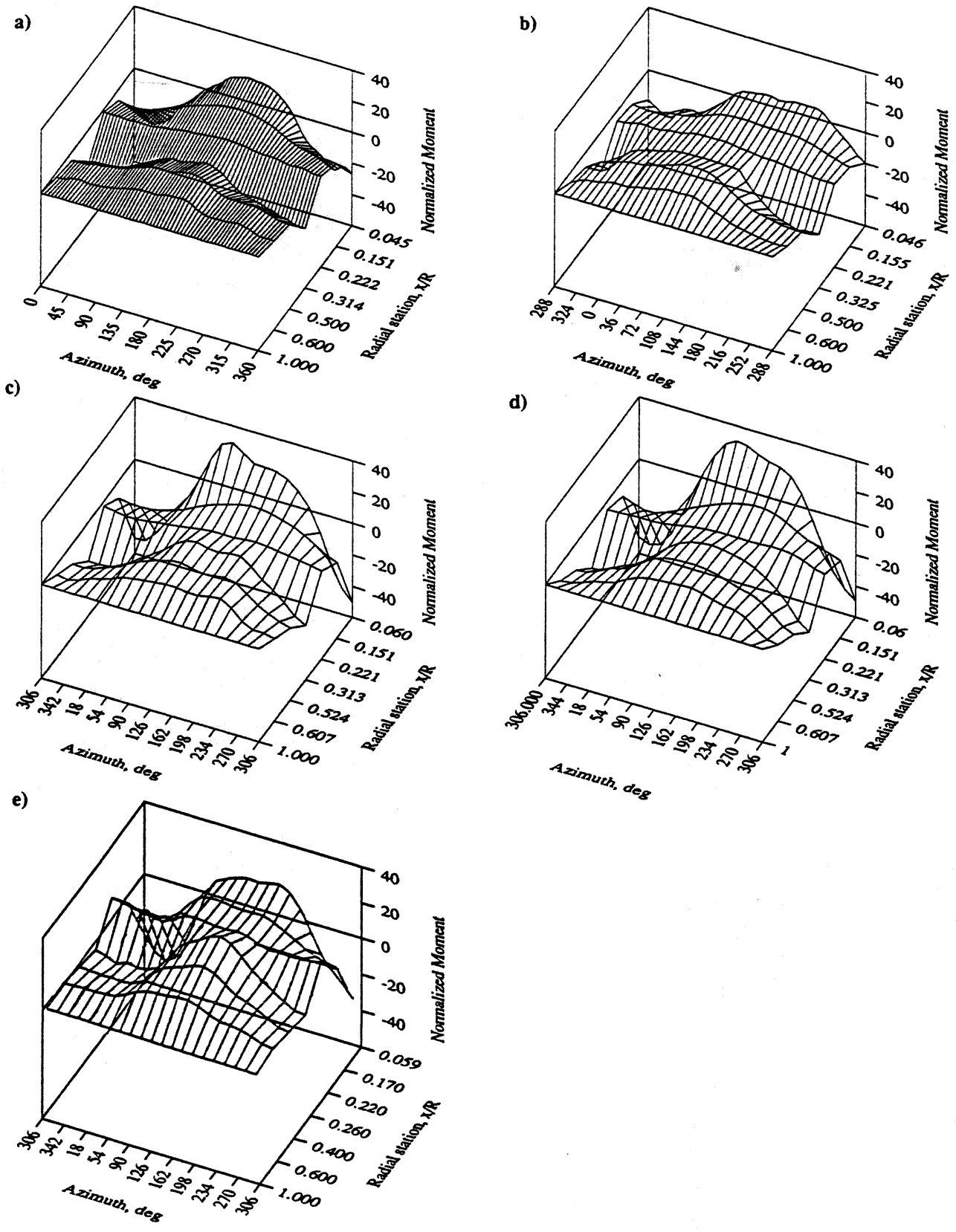

Figure 9. Chordwise bending moment, 100 knots, 14000 lb thrust, 315 RPM, a) measured, b) KTRAN (with free wake), c) UMARC/S modal method (with free wake), d) UMARC/S modal method (without free wake), e) UMARC/S force summation method (without free wake).

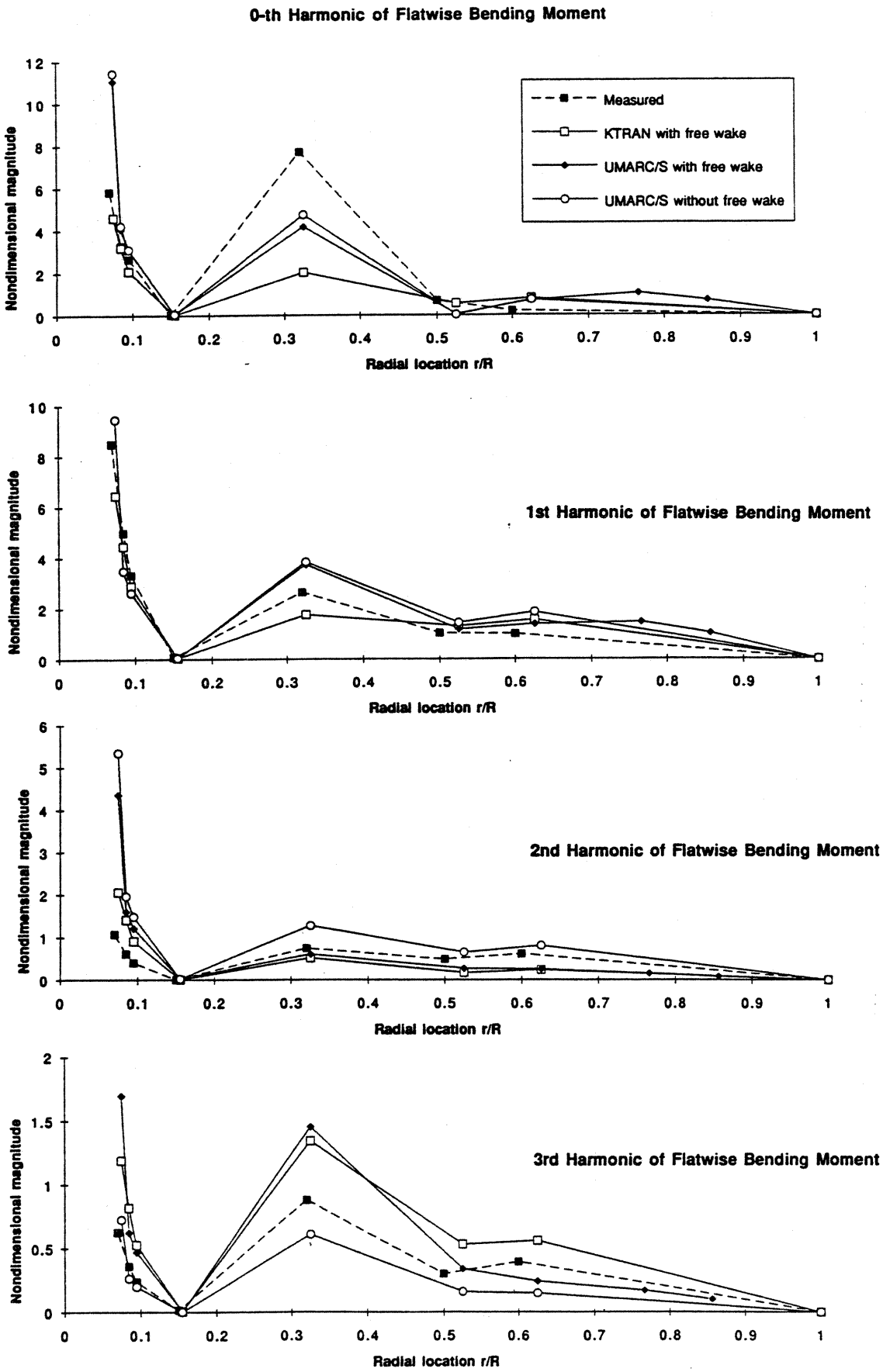

Figure 10a. Harmonic magnitude of flatwise bending moment, measured and predicted, 100 knots, 14,000 lb thrust, 315 RPM.

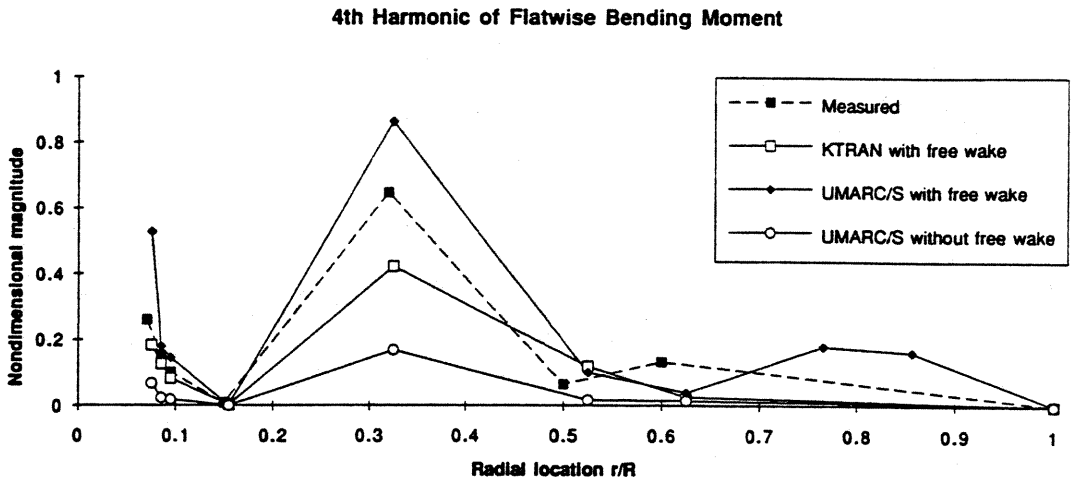

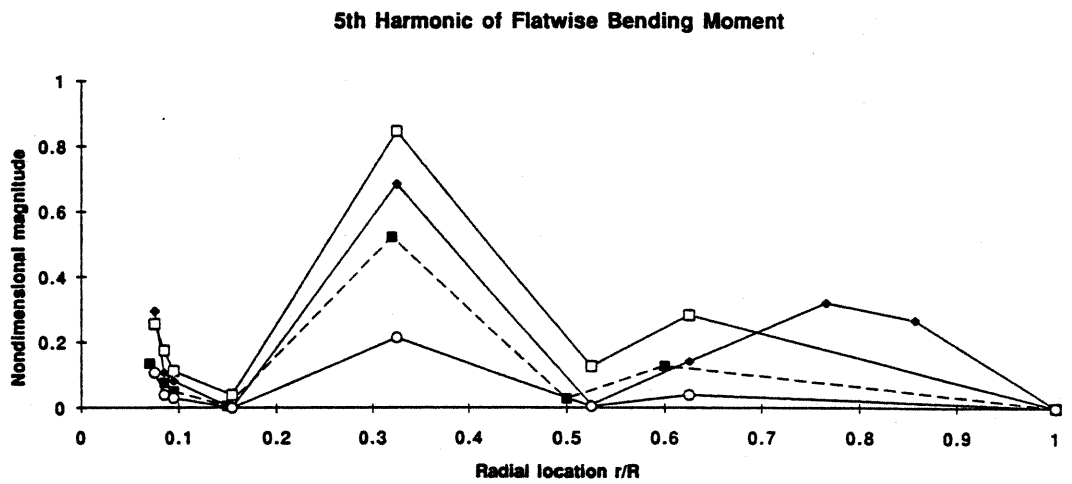

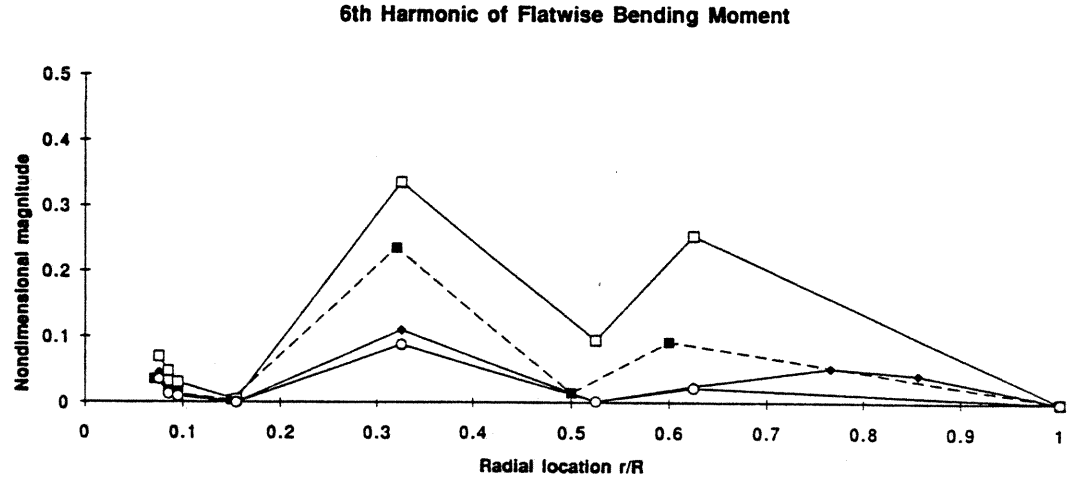

Figure 10a. (Continued)

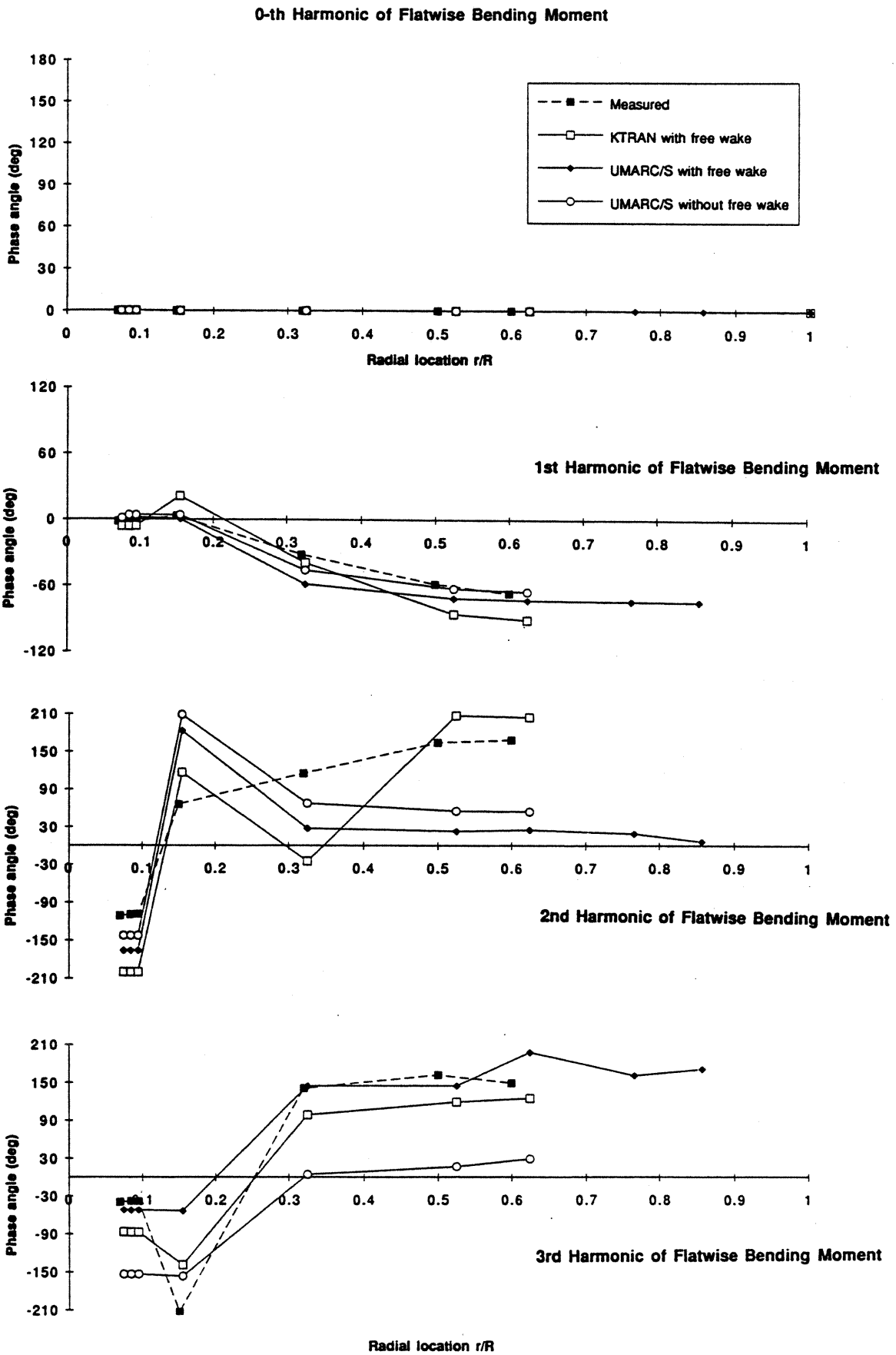

Figure 10b. Harmonic phase angle of flatwise bending moment, measured and predicted,100 knots, 14,000 lb thrust, 315 RPM.

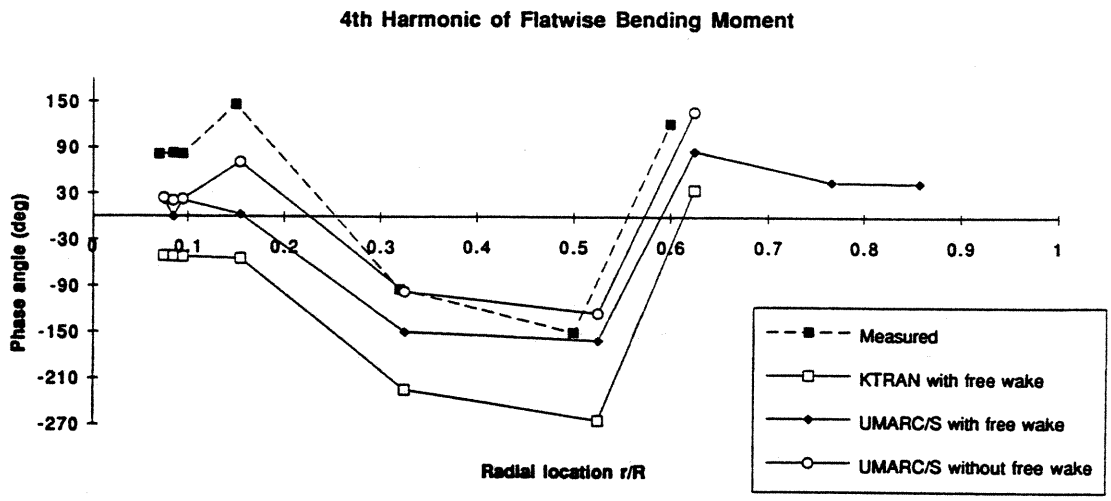

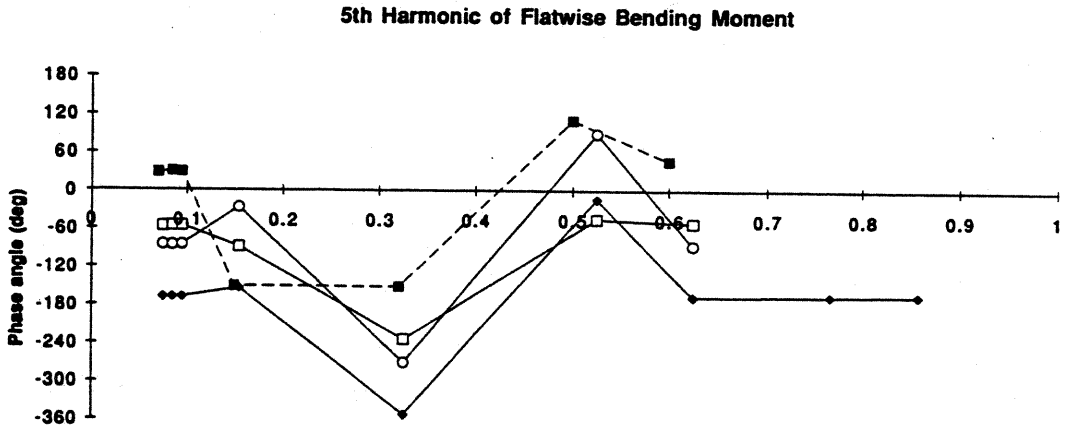

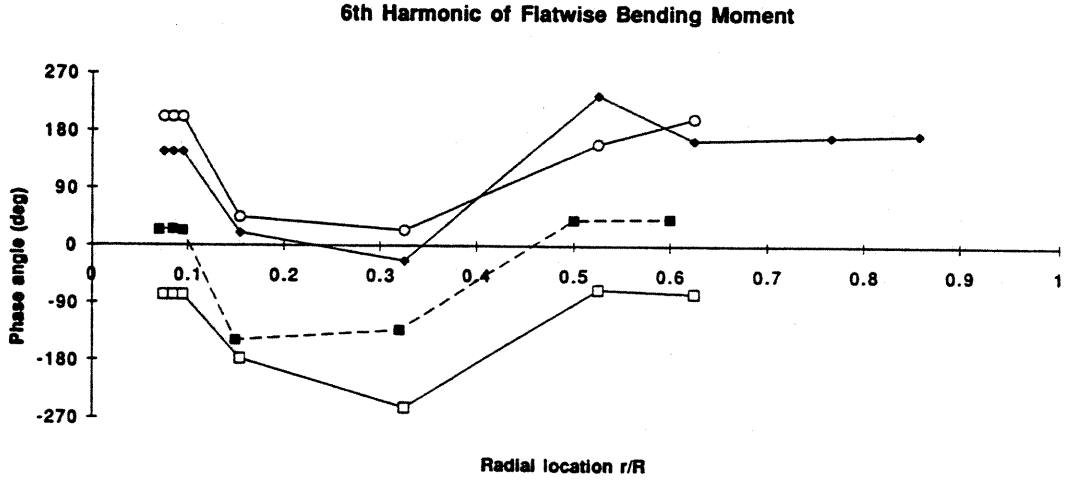

Figure 10b. (Continued)

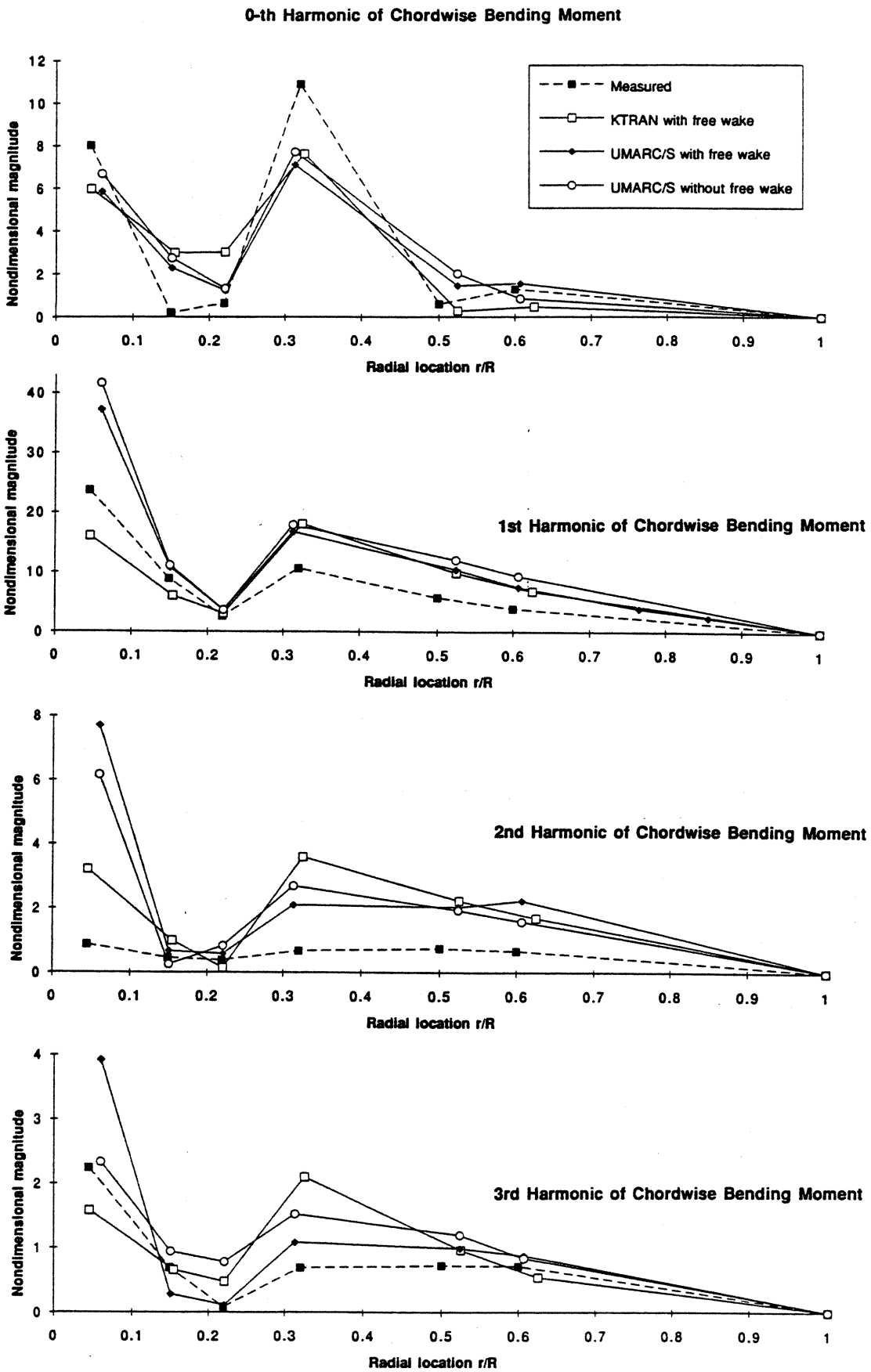

Figure 11a. Harmonic magnitude of chordwise bending moment, measured and predicted, 100 knots, 14,000 lb thrust, 315 RPM.

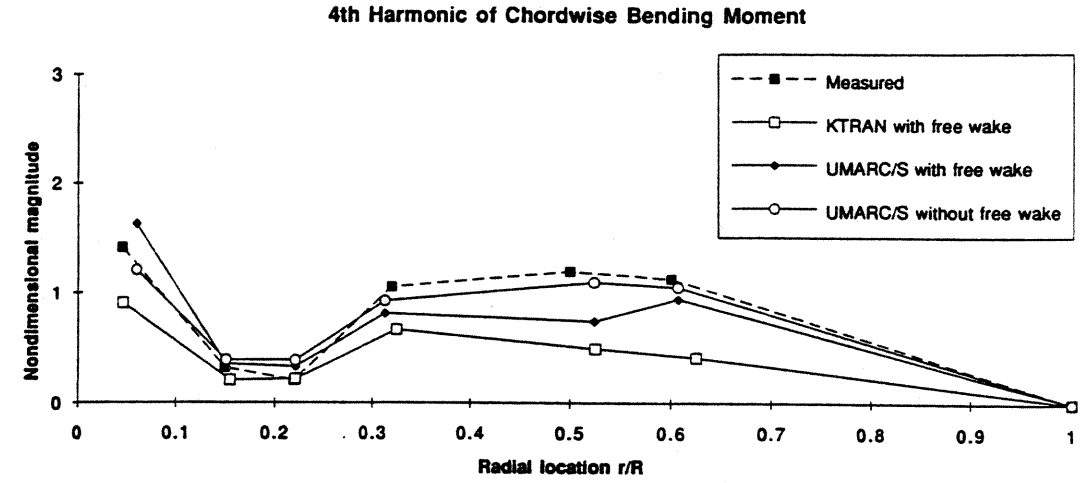

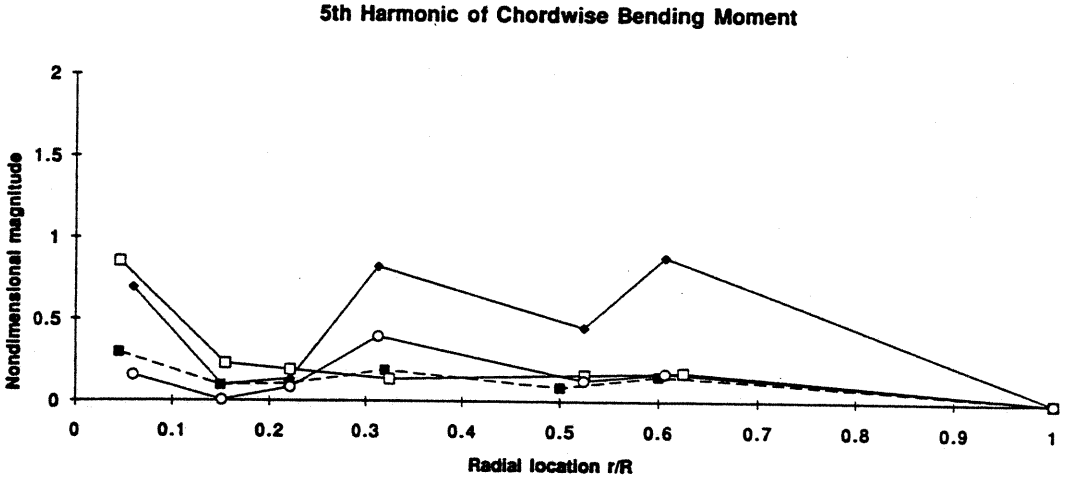

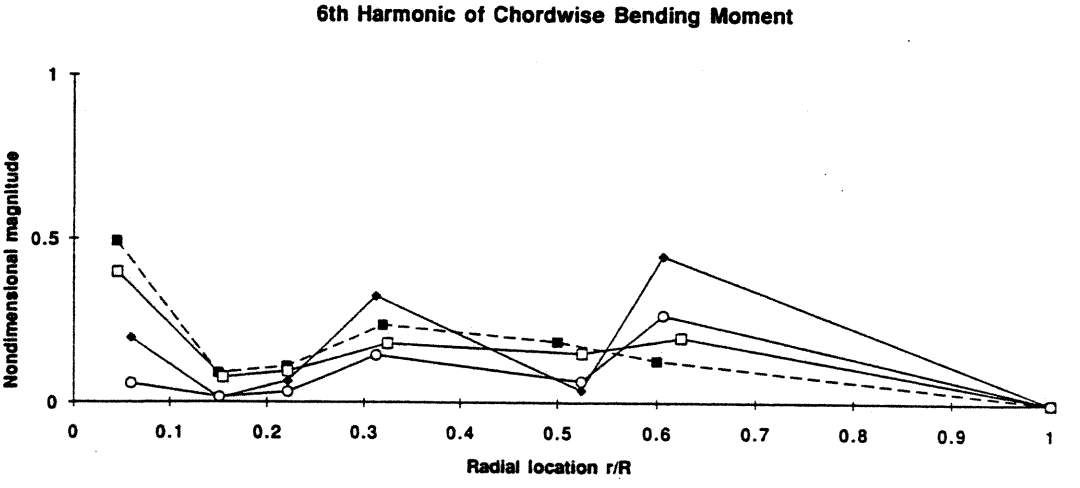

Figure 11a. (Continued)

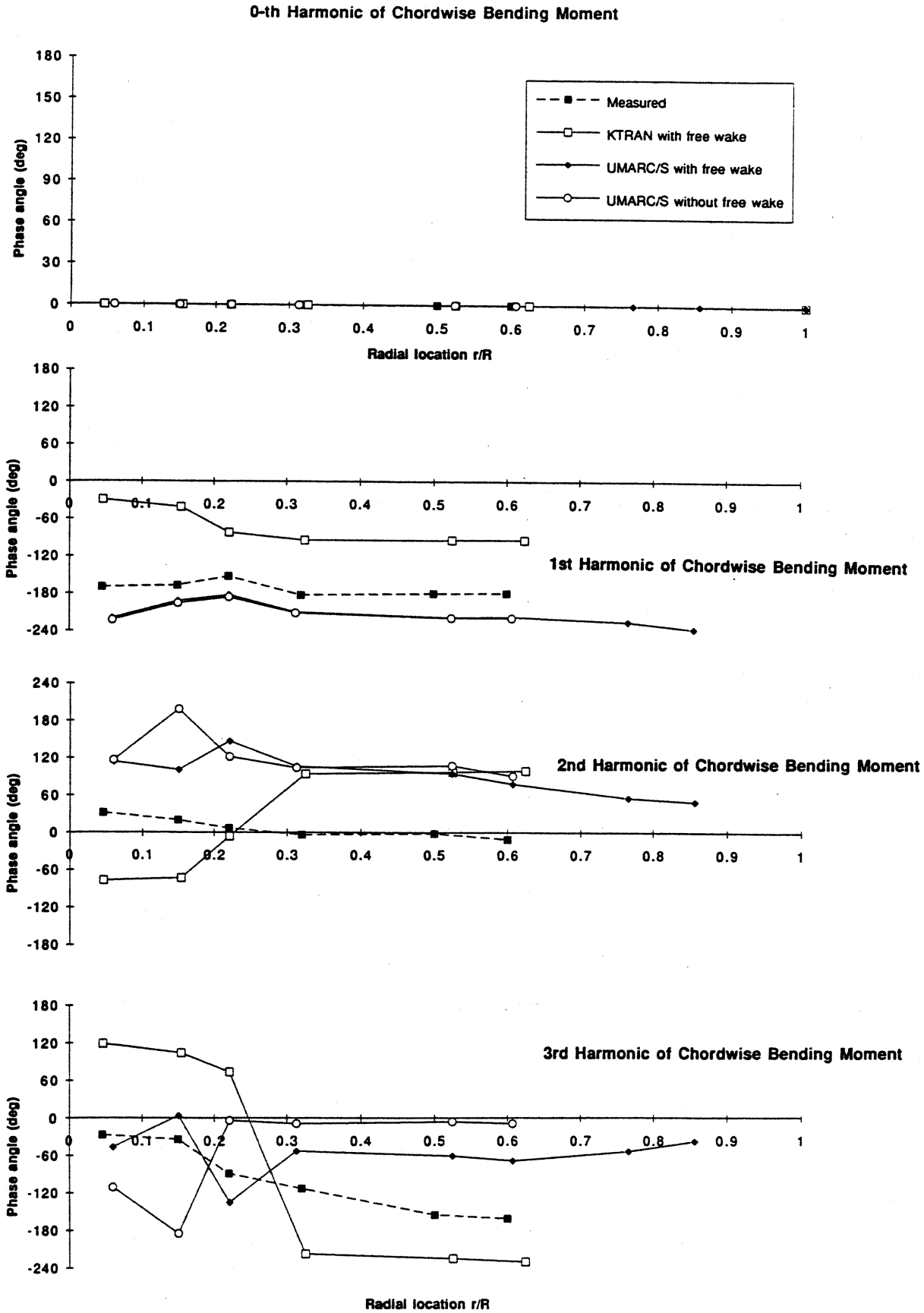

Figure 11b. Harmonic phase angle of chordwise bending moment, measured and predicted,100 knots, 14,000 lb thrust, 315 RPM.

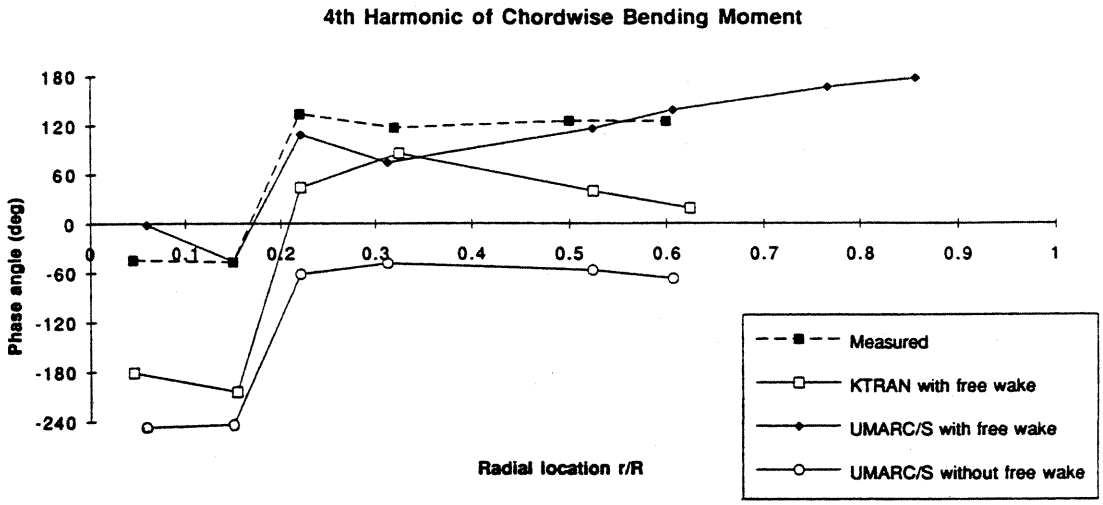

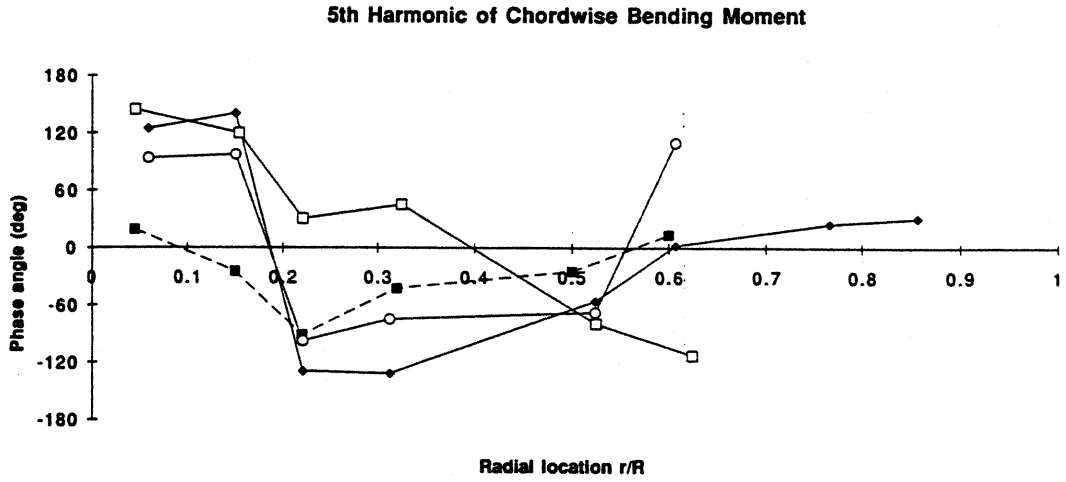

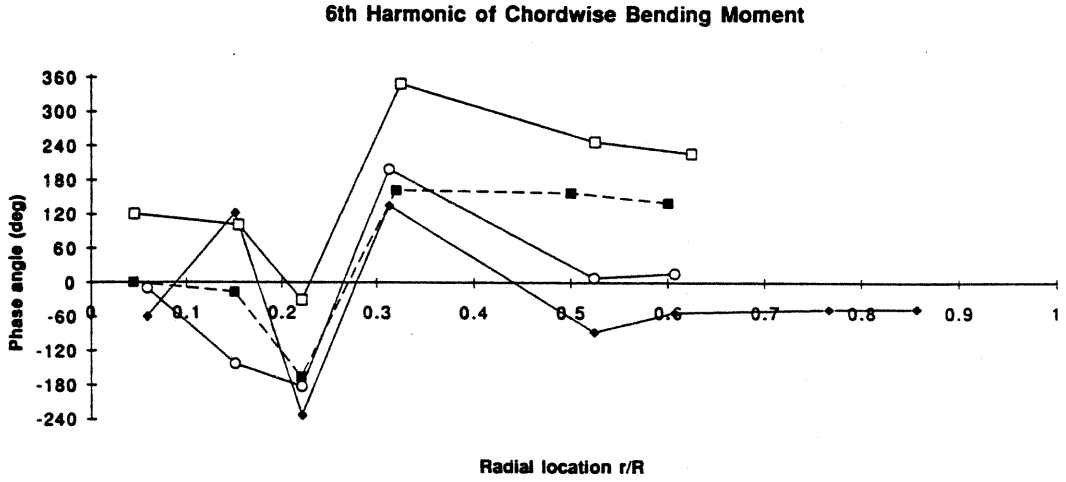

Figure 11b. (Continued)

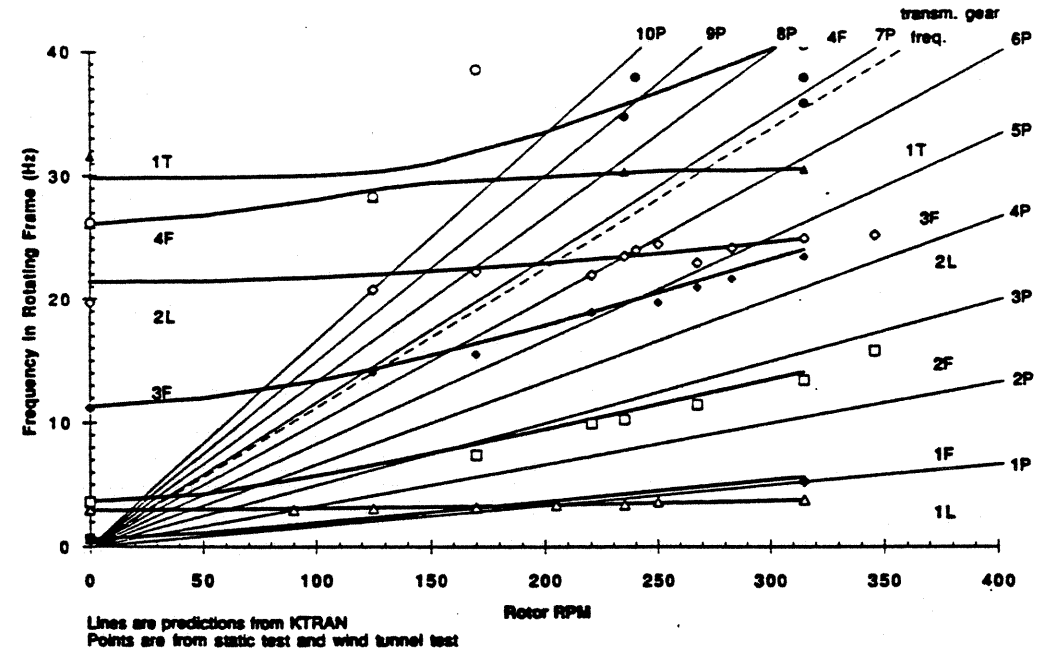

Figure 12. Measured and KTRAN-predicted Southwell frequency diagram.

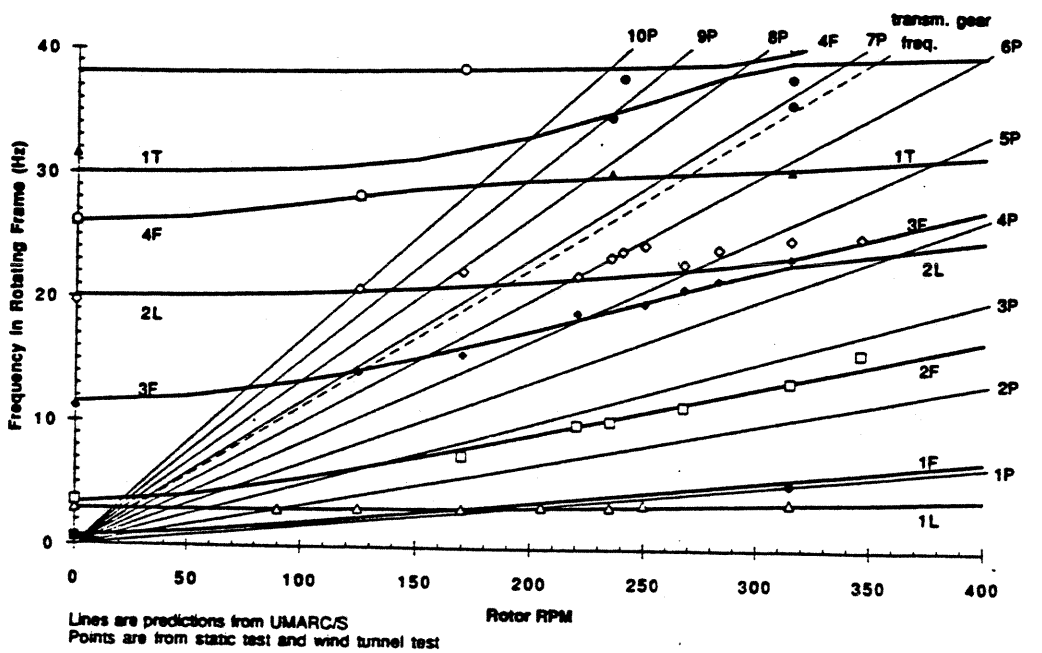

Figure 13. Measured and UMARC/S-predicted Southwell frequency diagram.

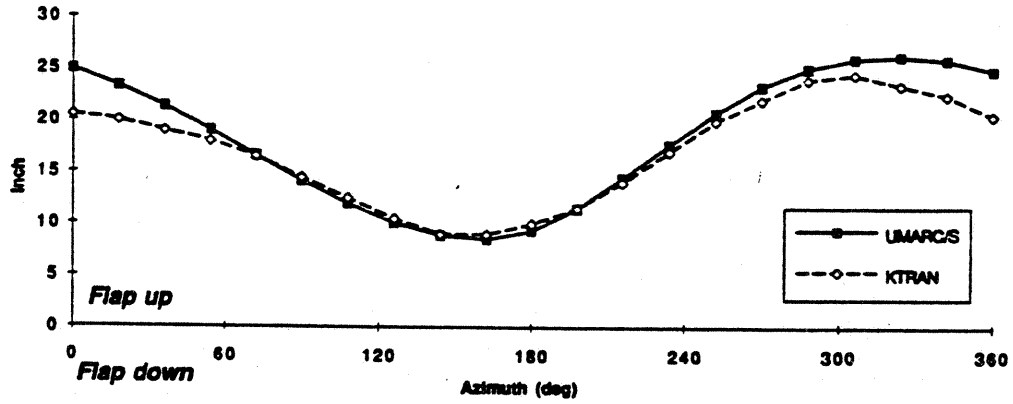

Figure 14. KTRAN and UMARC/S-predicted flap displacement at the blade tip, 100 knots, 14,000 lb thrust, 315 RPM.

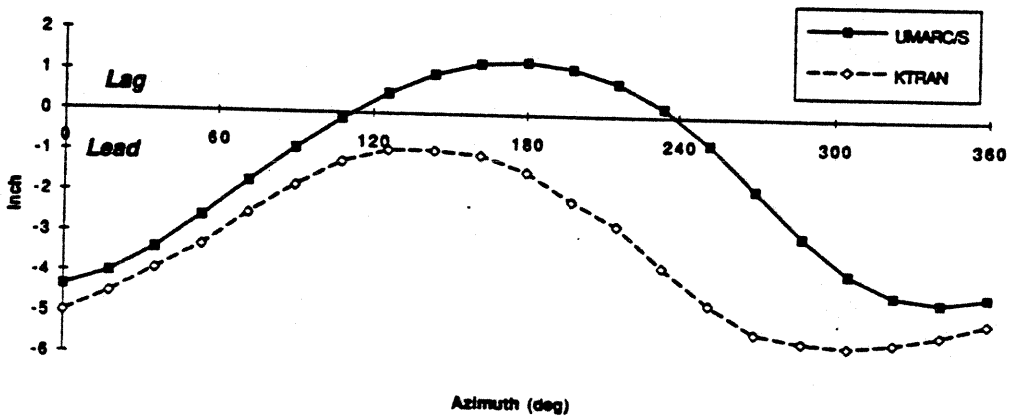

Figure 15. KTRAN and UMARC/S-predicted lag displacement at the blade tip, 100 knots, 14,000 lb thrust, 315 RPM.

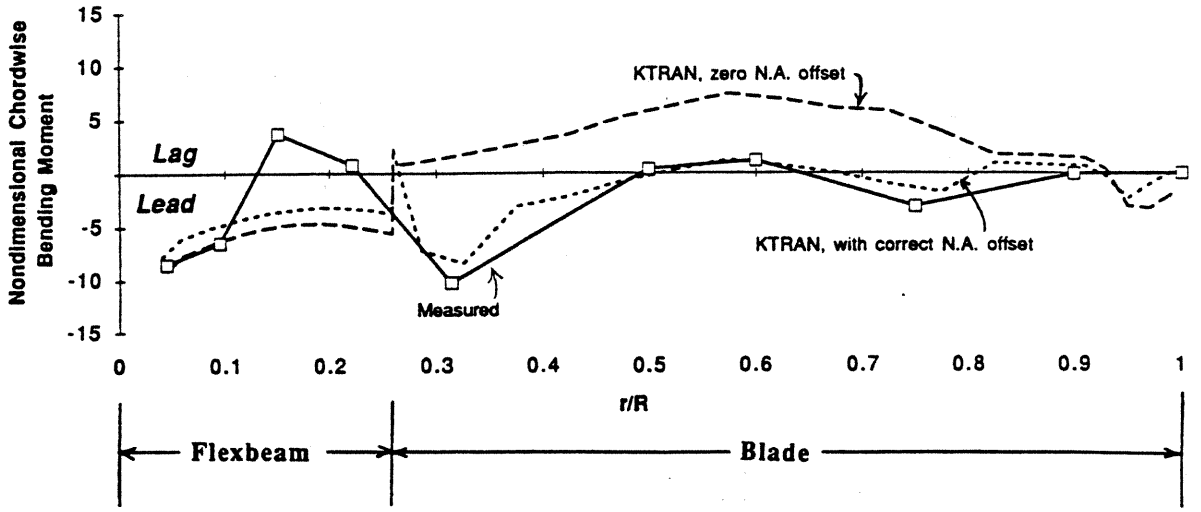

Figure 16. Effect of neutral axis modeling on steady chordwise bending moment, 80 knots, 14,000 lb thrust, 315 RPM.

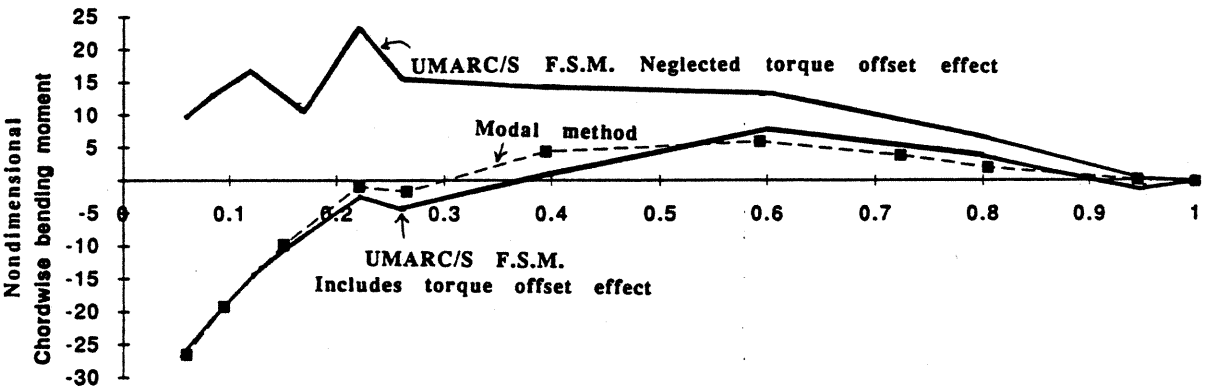

Figure 17. Effect of torque offset on steady chordwise bending moment when using force summation method, hover, C_T/σ = 0.001, 315 RPM, no precone. The redundant load path is accounted for in the force summation method.

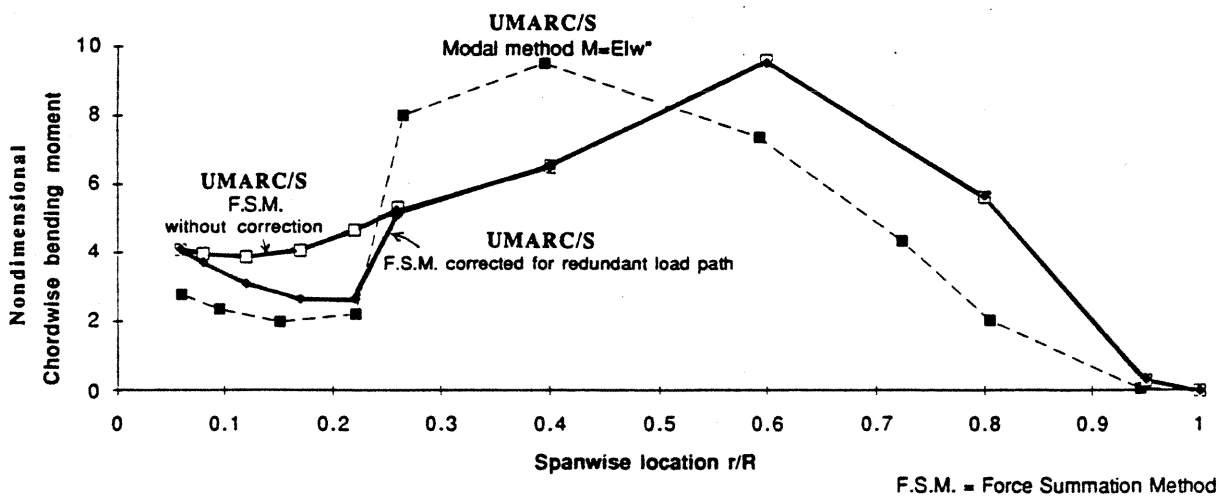

Figure 18. Effect of feedback loads from redundant load path on steady chordwise bending moment when using force summation method, hover, C_T/σ = 0.001, 315 RPM, no precone, no hub offset.

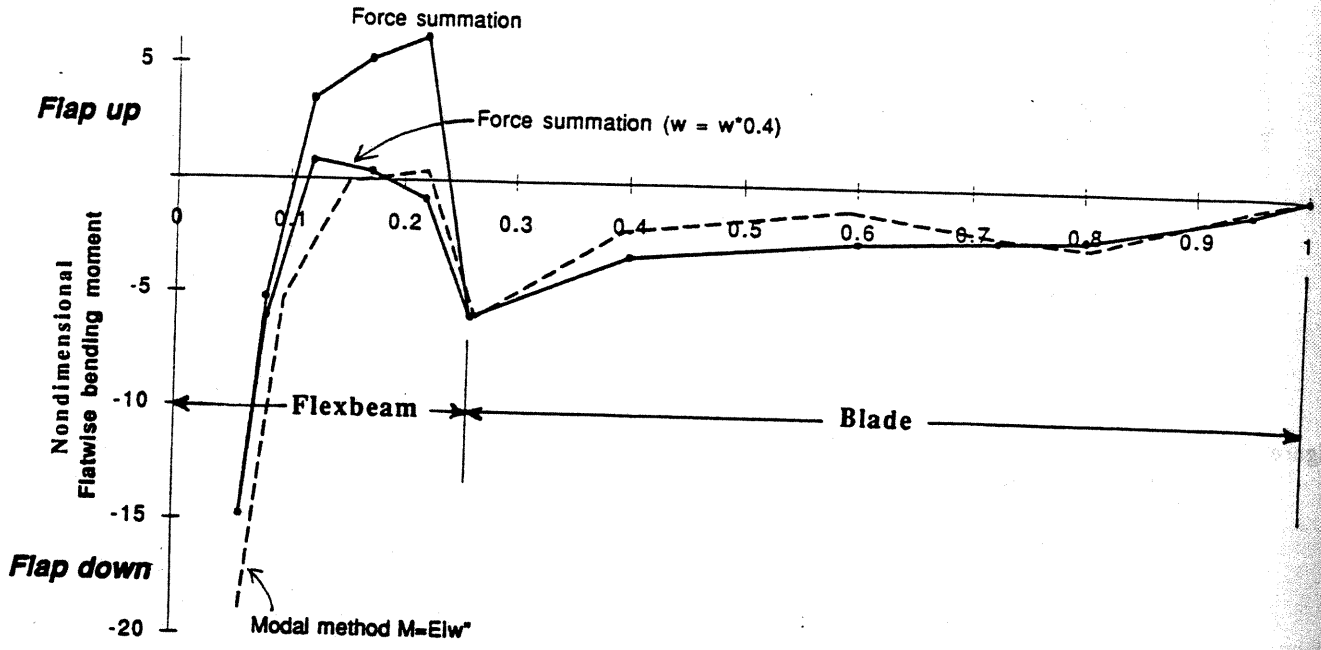

Figure 19a. Effect of feedback loads from redundant load path on flexbeam flatwise bending moment when using force summation method, hover, C_T/σ = 0.001, 315 RPM.

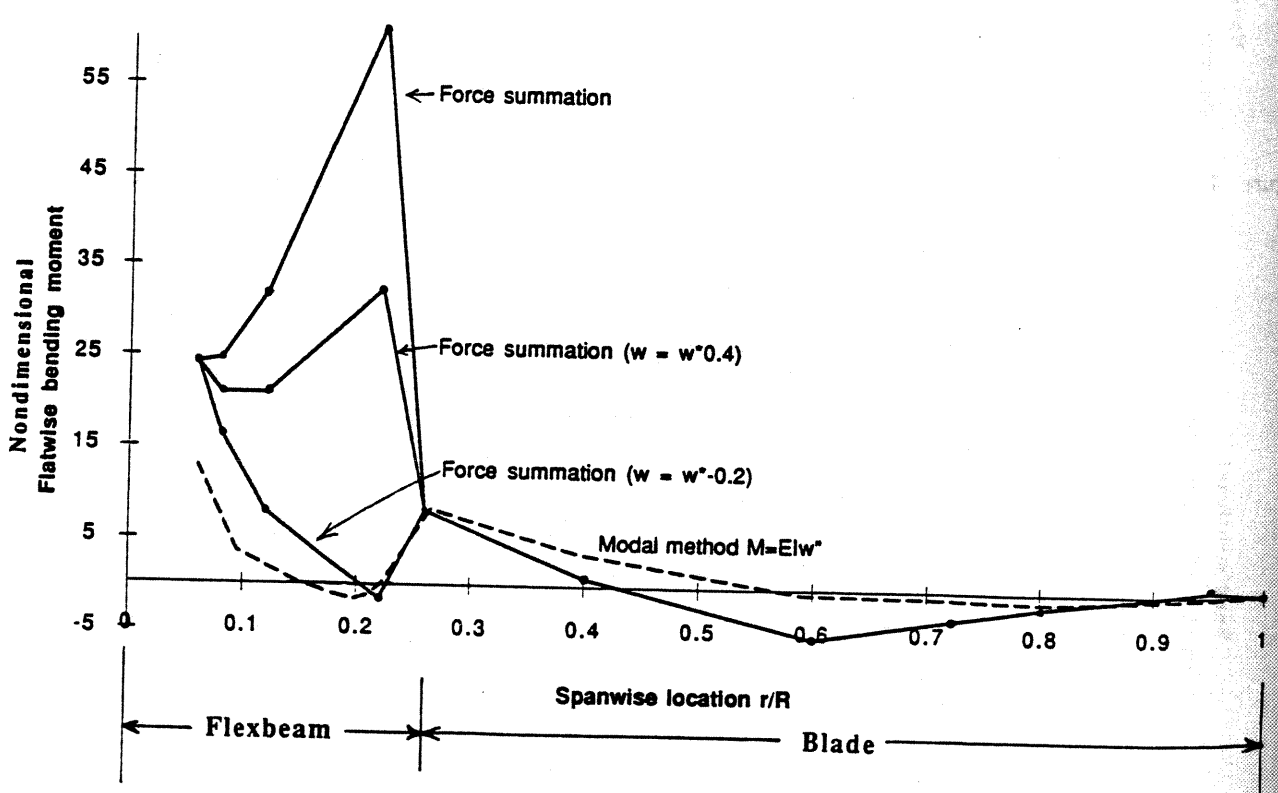

Figure 19b. Effect of feedback loads from redundant load path on flexbeam flatwise bending moment when using force summation method, hover, C_T/σ = 0.093,(14,000 lb thrust), 315 RPM .